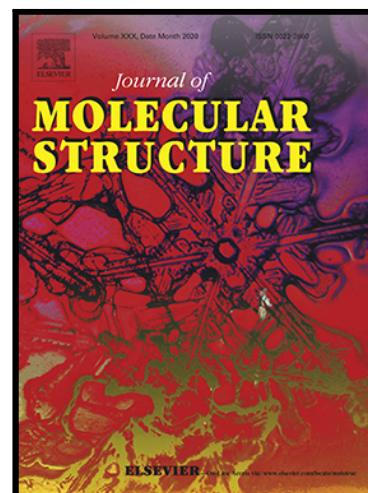


Journal Pre-proof

2-Amino-3-methylpyridinium, 2-amino-4-methylbenzothiazolium and 2-amino-5-chloropyrinium salts. Experimental and theoretical findings

Muhammad Hanif , Ezzat Khan , Muhammad Khalid ,
Muhammad Nawaz Tahir , Sara Figueirêdo de Alcântara Morais ,
Ataualpa Albert Carmo Braga

PII: S0022-2860(20)31239-4
DOI: <https://doi.org/10.1016/j.molstruc.2020.128914>
Reference: MOLSTR 128914



To appear in: *Journal of Molecular Structure*

Received date: 26 March 2020
Revised date: 12 July 2020
Accepted date: 15 July 2020

Please cite this article as: Muhammad Hanif , Ezzat Khan , Muhammad Khalid , Muhammad Nawaz Tahir , Sara Figueirêdo de Alcântara Morais , Ataualpa Albert Carmo Braga , 2-Amino-3-methylpyridinium, 2-amino-4-methylbenzothiazolium and 2-amino-5-chloropyrinium salts. Experimental and theoretical findings, *Journal of Molecular Structure* (2020), doi: <https://doi.org/10.1016/j.molstruc.2020.128914>

This is a PDF file of an article that has undergone enhancements after acceptance, such as the addition of a cover page and metadata, and formatting for readability, but it is not yet the definitive version of record. This version will undergo additional copyediting, typesetting and review before it is published in its final form, but we are providing this version to give early visibility of the article. Please note that, during the production process, errors may be discovered which could affect the content, and all legal disclaimers that apply to the journal pertain.

© 2020 Published by Elsevier B.V.

Highlights

Molecular salts of N-heterocyclic bases with salicylic and benzoic acid were obtained as crystals.

Molecular structure of three salts was determined by X-ray diffraction.

Non-covalent interactions in synthons have been discussed in details.

The AIM analysis of non-covalent interactions was carried out.

The O \cdots O, O \cdots S, Cl \cdots Cl, etc collaborate to direct the supramolecular arrangements.

Journal Pre-proof

2-Amino-3-methylpyridinium, 2-amino-4-methylbenzothiazolium and 2-amino-5-chloropyrinium salts. Experimental and theoretical findings

Muhammad Hanif^a, Ezzat Khan*^a, Muhammad Khalid*^b, Muhammad Nawaz Tahir^c, Sara Figueirêdo de Alcântara Morais^d, Ataulpa Albert Carmo Braga^d

^aDepartment of Chemistry, University of Malakand, Chakdara 18800, Khyber Pakhtunkhwa, Pakistan

^bDepartment of Chemistry, Khwaja Farid University of Engineering & Information Technology, Rahim Yar Khan-64200, Pakistan

^cDepartment of Physics, University of Sargodha, 40100 Punjab, Pakistan.

^dDepartamento de Química Fundamental, Instituto de Química, Universidade de São Paulo, Av. Prof. Lineu Prestes, 748, São Paulo, 05508-000, Brazil

Corresponding author's E-mail address: ekhan@uom.edu.pk (Prof. Dr. Ezzat Khan),

muhammad.khalid@kfueit.edu.pk; Khalid@iq.usp.br (Muhammad Khalid)

Abstract

Reaction between 2-amino-3-methylpyridine, 2-amino-4-methylbenzothiazole with salicylic acid, and 2-amino-5-chloropyridine with 3-chlorobenzoic acid were carried out and respective molecular salts **1-3** were obtained. During reactions proton transfer from acid to endocyclic N of the base was observed. Structural elucidation of all compounds was carried out with the help of FT-IR and X-ray Diffraction for single crystals. The acid/base pairs in a molecular salt are held together with the help of H- and charge assisted bonding and additional non-covalent bonding extend the supramolecular structure. All hydrogen bonds and secondary interactions have been discussed and a detailed comparison of experimental data with theoretical calculations through AIM, NBO and Wiberg bond index analysis has been made. The non-covalent character was mainly typified by positive values of Laplacian of electronic density. The theoretical studies demonstrate that other than classical H-bonds, the non-classical and secondary non-covalent interactions are very important to direct supramolecular structure of the respective molecular salt. The DFT calculations with solvent model SMD proved a good alternative to deduce the molecular salt formation when the $0 > \Delta pK_a > 3$. Moreover, global reactivity descriptors (GRD) have been calculated utilizing the energies of FMO. The calculated values for HOMO of compounds **1-3**, -5.469, -5.642 and -6.435, respectively indicate that the compounds adopt the numerical order in terms of electron donation/Lewis basicity. The molecular salt formation is more feasible for heterosynthons **1** and least for **3**.

Keywords: Molecular salts; salicylic acid; 3-chlorobenzoic acid; 2-amino-3-methylpyridine; 2-amino-4-methylbenzothiazole; Secondary/noncovalent interactions.

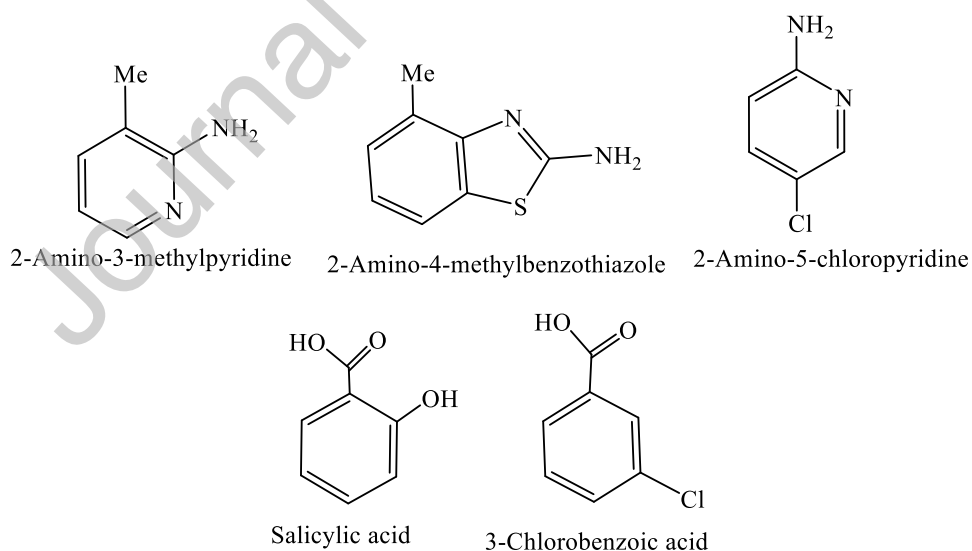
Introduction

Non-covalent interactions play a vital role in establishing supramolecular chemistry. The design and growth of functional materials is possible because of these interactions.[1, 2] These forces make the backbone of supramolecular chemistry and are consisting of classical and non-classical hydrogen bonding, electrostatic interactions and charge assisted/transfer interactions.[3-5] Intermolecular non-covalent interactions can be used as a key molecular recognition element in the multi-component crystalline systems. Multicomponent crystalline systems are classified into molecular salts, solvates and cocrystals. Many active pharmaceutical ingredients (APIs) with improved physical profile have been reported in the form of molecular salts, solvates and/or co-crystals.[6, 7] Hydrogen bonding is a significant non-covalent interaction and plays an important role in molecular recognition, crystal engineering, material science and biological systems.[8-10] It is also a significant driving force in organic salts in terms of its short separation distance, selectivity and directionality.[11-16] Generally hydrogen bonding interactions in molecular salts have shorter intermolecular distances as compared with those in co-crystals.[17, 18] Though molecular salts and co-crystals both can be described as multicomponent crystals but molecular salt can be distinguished from a co-crystal based on proton transfer from an acid to a base.[19, 20] The proton transfer depends upon the basicity and acidity of interacting functional groups that participate in hydrogen bond formation.[21, 22] An easy way for knowing the nature of multicomponent crystals comes from looking at the difference in pK_a values of acid and the base. "Rule of 3" is generally operative to predict the fate of multicomponent material, which categorize acid base pairs into two main groups. Pairs with $\Delta pK_a = pK_a(\text{base}) - pK_a(\text{acid}) > 3$ will undergo proton transfer and the resultant material are molecular salts. Similarly, if the value is less than 0, then co-crystal is the predominant product. All the components present in co-crystal do not alter in terms of their chemical structure and function.[23] However, the rule is improper for predicting molecular salt or co-crystal formation when the ΔpK_a value is between 0 and 3 [24] where both type of multicomponent compounds are possible. In this narrow region molecular salts and co-crystals overlap and the type of resulting complex appears to be random, signifying that pK_a is not a good predicting means in this region.[25] The molecular structure of acids and base and position of H-acceptor atom has to be considered in this regard.

The strategy of molecular salts is frequently used to modify certain properties like solubility, stability and hygroscopicity of a drug in the desired way.[14, 26] The carboxylic acid

functionality is very efficient in establishing the hydrogen bonding with a suitable base function and is therefore widely in practice in crystal engineering.[27] Besides acidic groups, CH₃, Cl, NO₂ groups are also active in constructing organic crystalline solids through non-covalent bonds.[28] It is remarkable to utilize the strong and directional identification of carboxylic acid with nitrogen containing molecules.[29-33] For this purpose the most commonly used bases are aminopyridine derivatives. Various molecular salts involving aminopyridine/carboxylate non-covalent interactions have been reported in literature recently.[34-37] 2-Aminopyridine and related bases possess wide spread applications including some medicinal applications[38] and supramolecular chemistry.[39] Such salts frequently lead to supramolecular systems which play an important role in crystal engineering.[40, 41]

A comprehensive literature survey reveals that behaviour of 2-amino-3-methylpyridine, 2-amino-4-methylbenzothiazole and 2-amino-5-chloropyridine particularly non-covalent interactions are unexplored. In continuation to our previous work[42] on non-covalent interactions in molecules, here such interactions between the above stated bases with salicylic acid and a chlorobenzoic acid (**Scheme 1**) are unexplored in solid state and the same have been theoretically reproduced and validated by DFT. An experimental and theoretical detailed study of non-covalent interactions is carried out.



Scheme 1. Starting synthons, three bases (upper) and two acids (lower) used in this study.

Experimental section

General consideration and spectroscopic studies

Chemical reagents such as 2-amino-3-methylpyridine, 2-amino-4-methylbenzothiazole and 2-amino-5-chloropyridine, salicylic acid, acetic acid and 3-chlorobenzaldehyde are commercial products (TCI, Japan) and were used without further purification. Handling of chemicals was carried out in open air, at room temperature. The melting point of compounds was determined in sealed capillary tubes using Stuart SMP-10 (Japan) and are uncorrected. FT-IR spectra for KBr pellets were recorded by SHIMADZU FT-IR Model 18400, in the range 4000-400 cm^{-1} . Single X-ray diffraction data (Mo-K α , $\lambda = 0.71073 \text{ \AA}$) were collected by using Bruker kappa APEXII CCD diffractometer at room temperature. The crystal structure solution and refinements were accomplished by SIR97,[43] SHELXL97,[44] WinGX31[45] and PLATON.[46]

Syntheses of heterosynthones 1, 2 and 3

2-Amino-3-methylpyridinium 2-hydroxybenzoate (1)

Molecular salt, **1** was prepared by adopting the literature procedure,[37] by treating 2-amino-3-methylpyridine (0.313 g, 0.291 mL, 2.172 mmol) solution in 10 mL ethanol which was drop wise added to solution (EtOH) containing equimolar amount of salicylic acid (0.300 g, 2.172 mmol). The reaction mixture was heated to reflux for 4 h, and was allowed to cool to room temperature. White precipitates were separated by filtration, washed with EtOH and were dissolved in ethylacetate. The solution was allowed to evaporate slowly at room temperature, after several days colorless crystals in the solution were grown. Crystals were separated, melting point was determined and FT-IR and single X-ray data were collected. m. p. = 171-172°C; FT-IR data $\nu(\text{cm}^{-1}) = 3379\text{br}$, 3088br, 2975w, 1667s, 1578s, 1455s, 1252s, 1049m, 855s, 759s, 665s.

2-Amino-4-methylbenzothiazolium 2-hydroxybenzoate (2)

The proposed molecular salt **2** was prepared in the same way as molecular salt **1**, by treating 2-amino-4-methylbenzothiazole (0.2378 g, 1.448 mmol) and equimolar amount of salicylic acid (0.200 g, 1.448 mmol) in ethanol. The expected compound was obtained as white precipitates, which was dissolved in THF and crystals were obtained at room temperature in few days. m. p. = 181-182°C; FT-IR data $\nu(\text{cm}^{-1}) = 3166$, 3082, 2921, 2726 (overlapped broad), 1627s, 1595s, 1451s, 1350s, 1246s, 772s, 718s.

2-Amino-5-chloropyridinium 3-chlorobenzoate (**3**)

Reaction between 3-chlorobenzaldehyde (0.5466 g, 3.889 mmol, in 10 mL ethanol) and 2-amino-5-chloropyridine (0.5000 g, 3.889 mmol) in the presence of 2 mL acetic acid was carried out with the intent to get the respective Schiff base, under 6 h reflux conditions. During the course of reaction, oxidation of aldehyde lead to *in situ* formation of 3-chlorobenzoic acid which further reacted with 2-amino-5-chloropyridine *via* proton transfer to afford corresponding molecular salt, **3**. The clear solution was allowed to stand at room temperature wherein after few days colourless crystals were grown, separated and studied. m.p. = 128-130°C; FT-IR data ($\nu(\text{cm}^{-1})$) = 3196w, 3070w, 2980w, 2752w, 2357m, 2355m, 1666s, 1481s, 1419s, 1354 s, 1149m, 846s, 738s, 655s.

Theoretical studies

To analyze the intermolecular interactions in the molecular salts **1-3**, theoretical calculations using Density Functional Theory (DFT) were performed. The DFT calculations were carried out using Gaussian 09[47] package with functional B3LYP-D3[48-50] and basis set 6-311+G(d,p)[51-53] by implicit solvent SMD model with ethanol as solvent. Structures of molecular salts **1-3** were obtained from their respective crystallographic information files (CIFs). Single point calculations (in gas phase) of structures **1**, **2** and **3** and their respective dimers were performed to analyse the non-covalent interactions in the packed structure of the crystals. Furthermore, optimization calculations (gas phase and with implicit solvent SMD model) of structures **1-3** were also performed to analyse the intermolecular interactions, especially the hydrogen bonds. The time-dependent DFT applying the TD-B3LYP-D3/6-311+G(d,p) method was used to calculate the global reactivity parameters. The non-covalent interactions were analysed through topological analysis using the Quantum Theory of Atoms in Molecules (AIM)[54, 55] and natural bond orbitals (NBO) analyses.[56] The AIM analysis of structures **1-3** were carried out using AIM, all package (Version 19.10.12)[57] from their wave function file (wfx), obtained from their calculations (optimization and single point) performed with Gaussian 09 package. The NBO analysis was performed to evaluate their intermolecular interactions of compounds **1-3** and the NBOs were calculated with Gaussian 09 using NBO Version 3.1 and the surfaces were plotted with ChemCraft package.[58]

Results and discussion

2-Amino-3-methylpyridine, 2-amino-4-methylbenzothiazole and 2-amino-5-chloropyridine possess pK_a values 7.24, 4.7 and 4.67, respectively. These bases bear two potential nucleophilic centres wherein at least one can be proton acceptor. These sites are easily accessible to establish such interactions with a suitable reagent particularly an acid to afford heterosynthons. We have recently reported the behaviour of analogous base derivatives with terephthalic acid, where molecular salts were exclusively obtained.[37] The carboxylic acids particularly benzoic acid derivatives have contributed tremendously towards the designing of multicomponent crystals. They have been used to improve poor profile of APIs. We dealt with several bases as ligands bearing at least two nucleophilic centres to explore the efficiency of these centres for their coordinating ability. In this regard we have reported a number of metal complexes wherein the endocyclic N has been proved to be more reactive/basic than the exocyclic N atom.[59-61] While ligating property of endocyclic N (aromatic) was found to be less than phosphorus (P) in other derivatives.[62] The basicity of various groups present in the same molecule was explored with selected two acids salicylic acid ($pK_a = 2.98$) and 3-chlorobenzoic acid ($pK_a = 3.82$). On the basis of “rule of 3” these pairs give $\Delta pK_a = 4.26$, 1.72 and 0.85 for 2-amino-3-methylpyridine/salicylic acid, 2-amino-4-methylbenzothiazole/salicylic acid and 2-amino-5-chloropyridine/3-chlorobenzoic acid pairs, respectively. The heterosynthons were expected to be molecular salt, for Acid/Base pair (hereafter denoted by A/B pairs) where the difference was greater than 3 and cocrystals for other A/B two pairs. We exclusively obtained molecular salts for all three A/B pairs, aiming to get deeper insights in the validity of the above stated rules.

Vibrational studies

The FT-IR data of compounds **1-3** (spectra given at the end of supporting file) indicate that molecular salts have been afforded as a result of proton transfer from acid to base. The presence of NH_2 group of the amine moiety indicates that this group is intact and does not accept proton because of its less basicity. All molecules **1-3**, show stretching bands in the range 3000-3100 cm^{-1} , which correspond to CH bonds.[63] In our study the IR bands at 3088 cm^{-1} in molecular salt **1**, at 2921 cm^{-1} in molecular salt **2** and at 3070-2895 cm^{-1} in **3**, correspond to aromatic C-H stretching vibrations. The C-H stretching vibration of methyl group in salt **1**

appears at 2975 cm^{-1} and in salt **2** at 2855 cm^{-1} . According to literature study the N-H stretching as a typically broad appears in the range of $3500\text{-}3200\text{ cm}^{-1}$. [64] The N-H stretching was observed at 3302 cm^{-1} in salt **1**, at $3082, 3030\text{ cm}^{-1}$ in salt **2** and at 3210 and 3196 cm^{-1} in salt **3**. There is observed a broad absorption at 3379 cm^{-1} in salt **1** and at 3166 cm^{-1} in salt **2** associated with stretching vibration of OH group in these compounds. Shift in the vibrational frequencies of some CH bonds, NH and OH reveal their involvement in secondary interactions, leading to supramolecular structure. Similarly literature study shows that C=C stretching of aromatic ring is mostly observed in the range $1610\text{-}1558\text{ cm}^{-1}$. [65] The C-S stretching vibrations are normally observed in finger print region in the expected range of $800\text{-}600\text{ cm}^{-1}$. [66] In this study, bands at 1578 cm^{-1} in salt **1**, at 1595 cm^{-1} in salt **2** and at 1539 cm^{-1} in salt **3** can be assigned to C=C stretching of aromatic rings. In salt **2** the C-S stretching vibrations appears at $772\text{-}718\text{ cm}^{-1}$. The strong peak appearing at 738 cm^{-1} was assigned to C-Cl stretching in salt **3**. Generally the carboxylate group (COO^-) shows two types of stretching, symmetric and asymmetric stretching in FT-IR spectrum. The symmetric stretching for carboxylate group is observed at $1425\text{-}1393\text{ cm}^{-1}$ while the asymmetric stretching appeared in the region of $1605\text{-}1585\text{ cm}^{-1}$. [67] In molecular salt **1** symmetric stretching frequencies of C-O appeared at 1610 cm^{-1} while the asymmetric stretching frequency appeared at 1667 cm^{-1} . In molecular salt **2** symmetric stretching appeared at 1627 cm^{-1} while the asymmetric stretching at 1680 cm^{-1} . Similarly in molecular salt **3** symmetric stretching of C-O appeared at 1665 while asymmetric at 1666 cm^{-1} . These stretching vibrations of carboxylate group (COO^-) confirms the molecular salts formation by proton transfer from carboxylic functional group (COOH) to endocyclic nitrogen of aromatic ring of amine derivatives. The least difference in symmetric and asymmetric frequencies of CO groups indicate that the electron density is equally distributed within the OCO fragment, giving almost uniform C-O bond in terms of strength.

Single crystal structure description of 1-3

Crystal structure solution and refinements parameters pertaining to compounds **1-3** are summarized in Table 1. Compound **1** crystallizes as monoclinic system in the space group $P2_1/c$. The asymmetric unit of compound **1** is composed of a cation of 2-amino-3-methylpyridinium and an anion of 2-hydroxybenzoate, thus affording a molecular salt, as shown in Figure 1. The molecular structure clearly indicates proton transfer from acid to the base. In the base unit a comparison of N nucleophilic centres (endo- and exocyclic) shows that aromatic N is more basic

thus accepting proton from the counter acid molecule. There are three oxygen atoms in the molecule of salicylic acid which give different bond lengths, worth explaining here for better understanding of difference in their chemical behaviour. The distance between C1-O1 is 1.271 Å, C1-O2 is 1.249 Å and between C3-O3 is 1.354 Å (Table S1). The separation distance between N1...O1 is 2.882 and between N2...O2 is 2.699 Å (see Table S1 for more details). Literature data regarding C-O distance in carboxylic acids fall in the region 1.237-1.245 and 1.265-1.273 Å, where slight variation can be explained because of intramolecular H-bonding. The bonding between acid/base pair is different than our recently reported compounds[37] where the interaction was established between $\text{H}_2\text{N}\cdots\text{O}=\text{C}$ and $\text{HN}^+\cdots\text{O}-\text{C}$ pairs, while in the instant compound **1**, the interaction has been found between $\text{C}-\text{O}\cdots\text{NH}_2$ and $\text{C}=\text{O}\cdots\text{NH}$ pairs. The data indicate that the electron density is partially delocalized on O1-C1-O2 fragment but still it is easy to decide that the negative charge is localized sufficiently on O1. The electron rich nature of O1 makes it suitable acceptor site for H-bonding, thus making an intramolecular hydrogen bonding with OH present at *ortho* position to it. Further, the same centre is also involve to establish a hydrogen bonding with NH_2 group of 2-amino-3-methylpyridine resulting the formation of a cyclic hydrogen bonded 8 membered ring, $R_2^2(8)$. This ring pattern is strong and is one of the 24 most regularly observed bimolecular cyclic hydrogen bonded ring in organic crystal structures.[8, 68, 69]

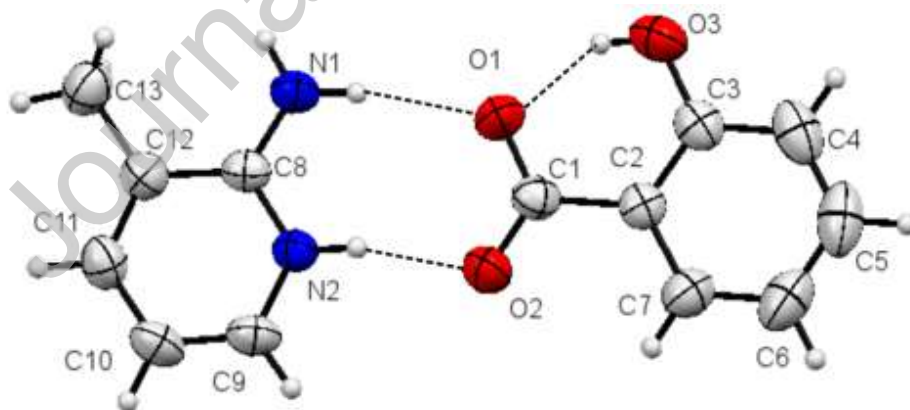


Figure 1. Crystal structure of compound **1**, thermal ellipsoids are drawn at 50% level, with numbering scheme for non-hydrogen atoms, Intramolecular and intermolecular hydrogen bonds are shown by dotted lines. Selected bond lengths and angles are given in Table S1. Proton transferred to N is shown in the molecule.

Hydrogen bonding in molecules of compound **1**, are given in Table S2, O3 and N1 play an important role in establishing a 1D supramolecular structure as depicted in Figure 2. The molecules containing $R_2^2(8)$ type ring units are linked together with the help of H-bonding between O3 and N1. The molecules are arranged in a parallel manner with a twist angle of 103° and are extended in a 1D fashion. The separation distance between two layers *i.e.*, O3...N1 is 3.038 Å. Some other short contacts between C9...O1, C9...O3 and C10...O2 are also present with a separation distance of 3.448, 3.170 and 3.549, respectively which extends the supramolecular structure in 2D fashion (not shown).

Table 1. Crystal refinements and solution parameters of compounds **1-3**

Compound	1	2	3
Empirical formula	C ₁₃ H ₁₄ N ₂ O ₃	C ₁₅ H ₁₄ N ₂ O ₃ S	C ₁₂ H ₁₀ Cl ₂ N ₂ O ₂
Formula mass	246.26	302.34	285.12
Crystal system	Monoclinic	Orthorhombic	Monoclinic
Space group	<i>P</i> 2 ₁ / <i>c</i>	<i>P</i> 2 ₁ 2 ₁ 2 ₁	<i>P</i> 2 ₁ / <i>c</i>
Temperature	296		
Unit cell parameters			
<i>a</i> (Å)	10.433(6)	6.970(11)	8.857(9)
<i>b</i> (Å)	8.903(5)	14.544(2)	11.755(9)
<i>c</i> (Å)	13.450(9)	14.570(3)	12.203(14)
α (°)	90	90	90
β (°)	103.277(2)	90	101.798(4)
γ (°)	90	90	90
<i>V</i> (Å ³)	1215.87(13)	1477.0 (4)	1243.6 (2)
<i>Z</i>		4	
<i>D</i> (g cm ⁻³)	1.345	1.355	1.523
μ (mm ⁻¹)	0.10	0.23	0.52
Crystal size	0.46×0.40×0.34	0.42×0.32×0.28	0.38×0.26×0.22

Absorption correction	Multi-scan		
R_{int}	0.038	0.041	0.094
Number of measured/ independent/observed	7583/2659/1790	8362/3217/2351	7787/2848/1994
Reflections [$I > 2\sigma(1)$]			
Number of reflection/ restraints/parameters	2659/0/165	3217/0/192	2848/0/172
Restraints/parameter			
$\Delta\rho_{\text{max}}, \Delta\rho_{\text{min}}$ ($e \text{ \AA}^{-3}$)	0.15, -0.15	0.14, -0.16	0.27, -0.30
Theta range ($^{\circ}$)	2.8 – 27.0	2.0 – 27.0	2.4-27.6
F(000)	520	628	584
$R[F^2 > 2\sigma(F^2)], wR(F^2), S$	0.045, 0.134, 1.04	0.043, 0.113, 1.01	0.049, 0.125, 1.04

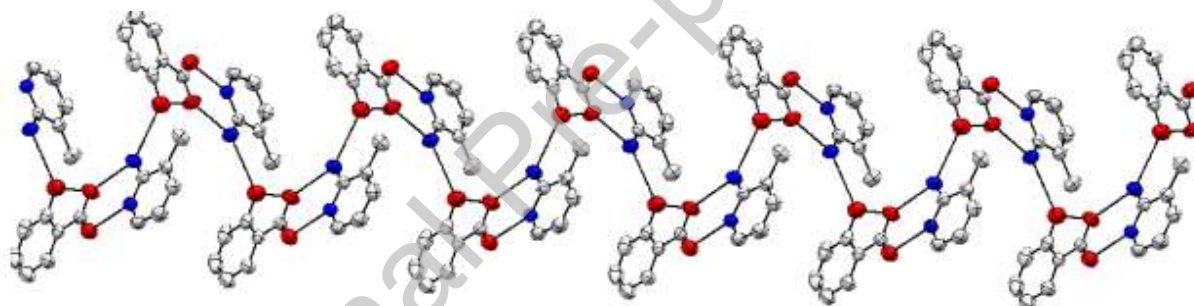


Figure 2. 1D supramolecular chain of compound **1**, stabilized by H-bonding between N1 and O3 of neighbouring acid/base pairs. The $R_2^2(8)$ type molecules in two layers chain are parallel with respect to each other. Hanging contacts, other short contacts and H-atoms are omitted for clarity.

Structural description of compound **2**

Molecular salt **2** with formula $[(2A4MBT)^+(SA)^-]$ crystallizes as orthorhombic colourless crystals in the space group $P2_12_12_1$. The structure of compound **2** with partial atomic numbering scheme is shown in Figure 3. Compound **2** reveals similar H-bonding as in compound **1**. The synthon (salicylic acid) undergoes proton transfer to 2-amino-4-methylbenzothiazole (2A4MBT)

where the endocyclic N acts as proton acceptor. Donor/acceptor atoms in reacting species interact to afford $R_2^2(8)$ ring system. The base molecule, 2-amino-4-methylbenzothiazole possesses three nucleophilic centres where both N are involved in H-bonding and charge assisted interactions, while S was not found to be involved in any sort of interaction as has been reported in several compounds reported by our research group.[59, 70, 71] The bond lengths C1-O1 1.244(4), C1-O2 1.261(4) and C3-O3 1.331(5), shown in Table S1, are slightly different than those in compound **1**. The electron density is relatively equally distributed over O1-C1-O2 fragment with a difference in C-O bonds equal to 0.017 Å in comparison to the difference of 0.022 Å in compound **1**. The C1-C2 distance is exactly equal to each other in both the compounds **1** and **2**. The C3-O3 bond is slightly shorter in comparison to compound **1**. All structural features of the counter molecule are very close to its structural analogue.[72]

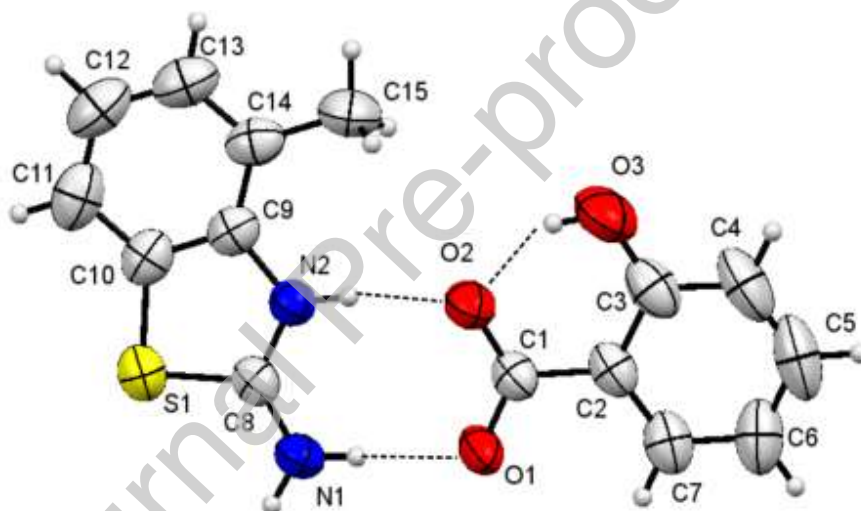


Figure 3. Molecular structure of compound **2**, with numbering scheme for C, N, S and O atoms, all hydrogen except N^+H are omitted for clarity, Hydrogen bonding (intramolecular and intermolecular) and charge assisted interaction are shown by dotted lines. For details pertaining to bond lengths and angles see Table S1 and S2.

The 2-amino-4-methylbenzothiazolium interacts with carboxylate group of 2-hydroxybenzoate ion *via* non-covalent interactions in the same way as in compound **1**. The C1=O1 of salicylic acid with slightly more double bond characters interacts with NH_2 group with a separation distance $O1 \cdots N$ 2.764 Å, and the same centres of the parallel layers are also linked together (2.751 Å). The C1-O2 bond and N2 are linked through charge assisted interaction CO^-

$\cdots\text{HN}^+$ separated by a distance of 2.715 Å (for detailed H-bonding see Table S3 and S4). These interactions stabilize the supramolecular structure in a 1D fashion as shown in Figure 4. There are several other interactions ($\text{C-H}\cdots\pi$, $\text{C-H}\cdots\text{O}$, $\text{N-H}\cdots\text{C}$, $\text{C-H}\cdots\text{C}$) which further cause to extend the structure in a 3D fashion. The S centre of benzothiazol moiety was not involved in any sort of interaction as has been reported in related studies[59, 73].

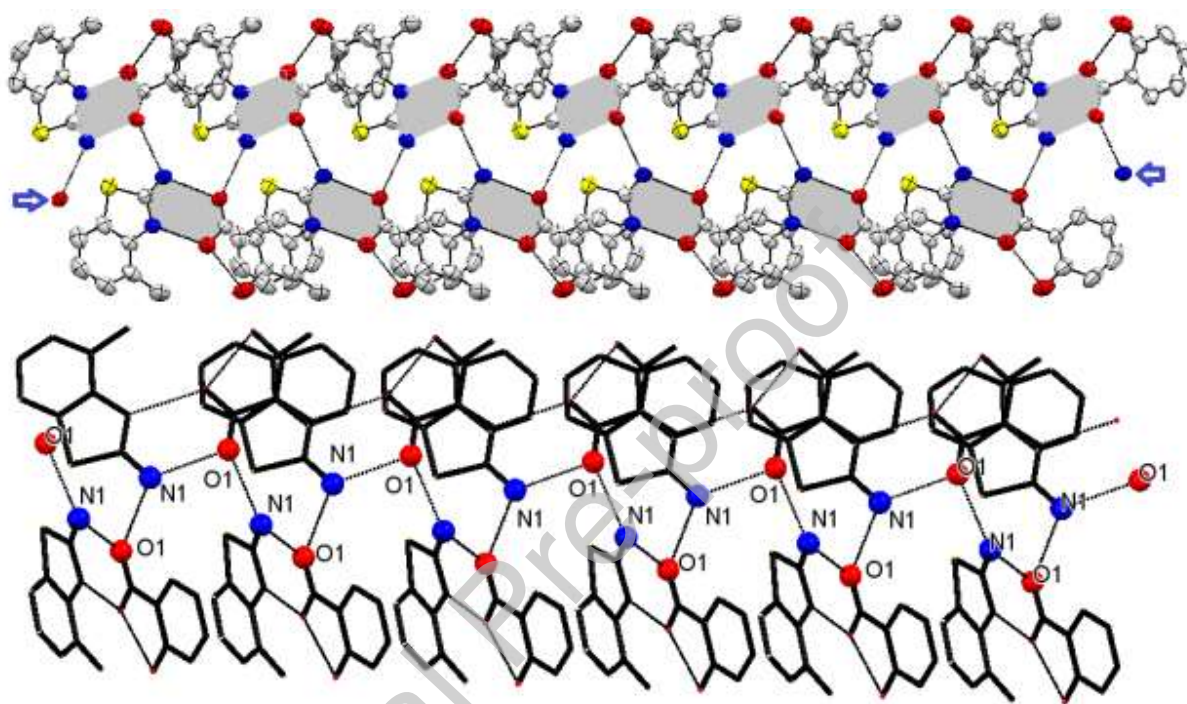


Figure 4. 1D chain of molecules of compound **2** stabilized through H-bonding (ellipsoid and capped sticks are given for easy understanding). The $R_2^2(8)$ rings are shown shaded in parallel layers of molecules for easy understanding.

Structural description of compound **3**

Compound **3** (molecular salt) was serendipitously obtained during the formation of a proposed Schiff base under aerobic conditions as discussed in experimental part (*vide supra*). The same molecular salt was successfully obtained in a reaction between the respective acid and the base. The molecule is monoclinic having space group $P2_1/c$. The compound **3** (as shown in Figure 5) consists of 2-amino-5-chloropyridinium and 3-chlorobenzoate ions. The proton transfer from 3-chlorobenzoic acid to the ring nitrogen atom of 2-amino-5-chloropyridine was observed. The same ring system as discussed above for molecular salts **1** and **2** was achieved for compound **3**

($R_2^2(8)$). Details pertaining to selected bond lengths and angles are given in Table S1 and S2 due to deprotonation, the resultant negative charge is distributed throughout the OCO fragment in a way to impart bond distances O1-C1 and C1-O2 1.238(3) and 1.271(2), respectively (see Table S1 for more details). Oxygen atom bonded to carbon in the latter case reveals comparatively more single bond characters thus indicating sufficient electron density (polarity). The O2 and N2 are associated with each other *via* charge assisted interaction ($\text{CO}^{\cdots+}\text{HN}$ 2.623 Å). Base-cation and acid-anion orient themselves in such a way that their additional donor/acceptor centres establish H-bonding thus affording a planar Base-Acid type molecular salt. The separation distance between $\text{O1}\cdots\text{N1}$ is 2.755 Å, the data clearly differentiate hydrogen bonded sites from charge assisted bound.

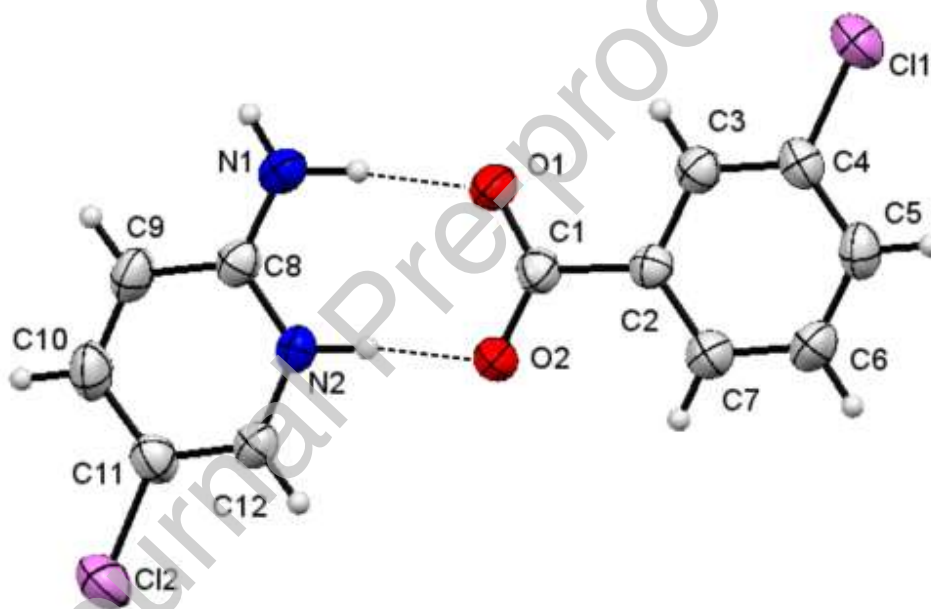


Figure 5. X-ray structure of Molecular salt **3** with complete numbering scheme (for non-hydrogen atoms), thermal ellipsoids are drawn at 50% probability level, hydrogen atoms are omitted for clarity and non-covalent interactions are shown by dotted lines.

Supramolecular structure of compound **3**, as a result of various secondary interactions is shown in Figure 6. The Acid/Base pairs are linked through H-bonding and charge assisted interactions in a molecular salt. Molecular salts or heterosynthons further interact with each other wherein both oxygen atoms are involved. The O1 is linked to Cl1 (3.240 Å) while O2 interacts

with N1 with a separation distance of 2.926 Å, Shown in Figure 6. Because of these interactions the supramolecular structure is stabilized in a 3D manner. Other noncovalent interactions were also found as were present in compounds **1** and **2**.

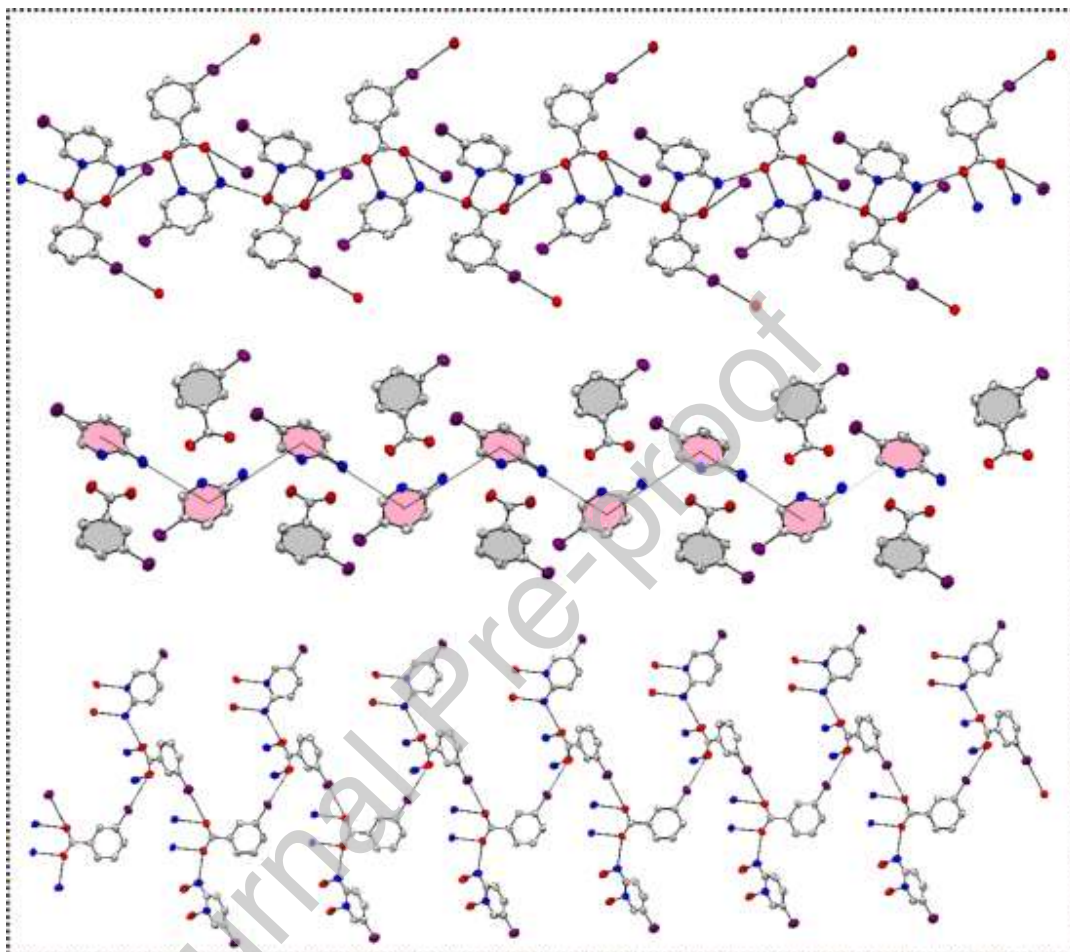


Figure 6 Chains of molecular salt **3**, stabilized by secondary interactions. On the top, molecular salts are linked through $\text{NH}\cdots\text{O}$ hydrogen bonding, $\text{O}\cdots\text{Cl}$ hanging contacts are also shown which extend the structure further. Middle, cations and anions are shown, where 2-aminopyridinium cations exist in a zigzag manner. Lower, acids moieties are linked via $\text{O}\cdots\text{Cl}$ and Acid/base pairs via $\text{O}\cdots\text{N}$ interactions. Selected hanging contacts are shown with each acid and base fragment.

Theoretical studies

The DFT based (B3LYP-D3/6-311+G(d,p)) optimized geometries of molecular structures (in gas and solvent phases) **1-3** were found in close agreement to their respective experimental

structures (Table S1-S4). The optimization in gas phase reveals that formation of molecular salt is predominant for **1** and **2**, while a cocrystal for compound **3**. However, the optimization with solvent model (SMD/DFT) indicates a salt formation for all structures **1-3**. Because of that, the optimized structural parameters with SMD/DFT were found in best agreement to experimental data. Therefore, the optimized geometries of structures **1-3** with SMD model were found more suitable hence used to calculate the global reactivity descriptors (GRDs) with TD-B3LYP-D3/6-311+G(d,p) method to evaluate the reactivity of the structures **1-3**.

The global reactivity descriptors were obtained applying the highest occupied molecular orbital (HOMO) and lowest unoccupied molecular orbital (LUMO) energies (in eV) of structures **1-3**, calculated with the following equations. The ionization potential (IP) and electron affinity (EA) were calculated using Eq 1 and Eq. 2. [74]

$$IP = -E_{\text{HOMO}} \quad \text{Eq. 1}$$

$$EA = -E_{\text{LUMO}} \quad \text{Eq. 2}$$

Koopman's theorem was used to calculate the global hardness (η)[75], electronegativity (X)[76] and chemical potential (μ)[77] with following equations:[78]

$$X = \frac{[IP + EA]}{2} \quad \text{Eq. 3}$$

$$\eta = \frac{[IP - EA]}{2} \quad \text{Eq. 4}$$

$$\mu = \frac{E_{\text{HOMO}} + E_{\text{LUMO}}}{2} \quad \text{Eq. 5}$$

The global electrophilicity index (ω) [79, 80] was calculated using the Eq. 6 reported by Parr *et. al.* as:

$$\omega = \frac{\mu^2}{2\eta} \quad \text{Eq. 6}$$

To calculate the global softness (σ) [81], Eq. 7 was used:

$$\sigma = \frac{1}{2\eta} \quad \text{Eq. 7}$$

The frontier molecular orbitals (FMO) analysis (Table 2) of structures **1-3** showed that the followed trend of $\Delta E_{\text{HOMO-LUMO}}$ gap is **1<3<2**. Frontier molecular orbitals (HOMO and LUMO) are important to the reactivity description of molecules. The HOMO values can demonstrate the electron donating characteristic while the LUMO energies demonstrate characteristic of electrons acceptance. Furthermore, higher $\Delta E_{\text{HOMO-LUMO}}$ indicate chemical stability. Thus, the observed trends of $\Delta E_{\text{HOMO-LUMO}}$ gap indicating a higher chemical stability for structure **2**, followed by **3** and **1**, respectively. Although, the structures **1-3** showed small energy differences in the FMO analysis characterizing them with similar chemical stability. The plot of HOMO and LUMO surfaces are shown in the Figure 7. The global reactivity descriptors (GRDs) calculated from HOMO and LUMO energies of structures **1-3** which are arranged in Table 3.

Table 2. Frontier molecular orbitals energies for structures **1-3**

Structures	MOs	Energy	ΔE
1	HOMO	-5.469	
	LUMO	-2.456	3.013
2	HOMO	-5.642	
	LUMO	-1.771	3.871
3	HOMO	-6.435	
	LUMO	-2.786	3.649

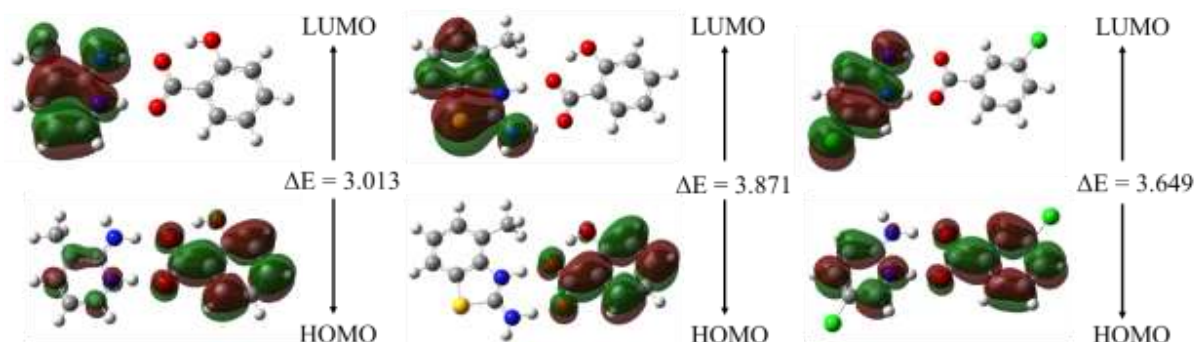


Figure 7 Frontier molecular orbitals calculated for structures **1-3**.

Table 3. Global reactivity descriptors calculated for structures **1-3**

Structures	IP	EA	χ	η	μ	ω	Σ
1	5.469	2.456	3.963	1.507	-3.963	5.211	0.332
2	5.642	1.771	3.707	1.936	-3.707	3.549	0.258
3	6.435	2.786	4.610	1.825	-4.610	5.824	0.274

Comparing the global reactivity descriptors (Table 3) among the structures **1-3** it was verified that the structure **3** has the higher ionization potential ($IP = 6.435$) followed by structures **2** and **1** ($IP = 5.642$ and 5.469 , respectively). Although the IP values demonstrate that compounds **1-3** possess larger stability and chemical inertness. A mutual comparison indicates that compound **3** possess higher stability than compounds **1** and **2**. Beyond that, the structure **3** also exhibits highest electronic affinity ($EA = 2.786$), than **1** and **2**, indicating that the structure **3** accepts electrons more easily than structures **1** and **2** ($EA = 2.456$ and 1.771 , respectively). The global electronegativity ($\chi = 4.610$) of structure **3** was also higher than structures **1** and **2** ($\chi = 3.963$ and 3.707 , respectively), which is expected due the presence of Cl atoms in the structure **3**. On the other hand, the global hardness descriptor of structure **1** (which has the higher energy gap i.e., $\Delta E_{HOMO-LUMO}$) showed higher value ($\eta = 1.936$) than structures **3** and **2** ($\eta = 1.825$ and 1.507 , respectively). Moreover, the structure **3** exhibited lowest global chemical potential value ($\mu = -4.610$) followed by structures **1** and **2** ($\mu = -3.963$ and -3.707 , respectively). That is, associated with the higher global electronegativity, the compound **3** exhibited a higher tendency to attract electrons and hold them firmly in comparison to structures **1** and **2**. The structure **3** also has higher global electrophilicity ($\omega = 5.824$) than structures **1** and **2** ($\omega = 5.211$ and 3.549 ,

respectively). Nevertheless, the structure **1** has ω value closer to **3** indicating that these compounds have higher electrophilic character than **2**. Finally, the structure **1** showed higher global softness value ($\sigma = 0.332$) than structures **3** and **2** ($\sigma = 0.274$ and 0.258 , respectively). Analysing the data as discussed is in the opinion that compound **1** is softest among the three.

AIM and NBO Analysis

Topological AIM analysis is widely used to characterize non-covalent interactions through the Quantum Theory of Atoms in Molecules (QTAIM) developed by Richard Bader.[55, 82, 83] The QTAIM is based on the topological analysis of electronic density $\rho(r)$, to describe the AIM properties such as presence and strength of non-covalent interactions in a molecule. In broad terms, the attractors (atoms) defines the distribution of gradient vector, $\nabla\rho(r)$, which establishes the fundamental conditions for topological analysis of molecular systems. The evaluation of Laplacian of electronic density, $\nabla^2\rho(r)$, curvature characterize the critical points (CP). Thereby, the trace of Hessian Matrix of density, $\text{Hess}(\rho) = \nabla^2\rho(r) = \frac{\partial^2\rho}{\partial^2x} + \frac{\partial^2\rho}{\partial^2y} + \frac{\partial^2\rho}{\partial^2z} = \lambda_1 + \lambda_2 + \lambda_3$ provides the CPs that are featured by rank (number of eigenvalues λ_n not null) and signature (sum of λ_n). The most important CP in our analysis is the bond critical point (BCP) with rank +3 and signature -1, a topological saddle point (+3,-1) between two attractors. The path lines that connect two attractors starting from same BCP is called bond path (BP) and it features an interaction between two attractors, which can be a bond (covalent or ionic), a non-covalent interaction etc. Moreover, negative Laplacian of density values ($-\nabla^2\rho(r)$) reveals converge of $\rho(r)$, which indicates covalent interactions, while the positive values of $\nabla^2\rho(r)$ reveals divergence of $\rho(r)$ and is an indication of charge separation at the BCP that can reveal charge assisted and other non-covalent interactions. Moreover, the ellipticity evaluates the electronic density distribution symmetry in the BCP, thus $\varepsilon = 0$ indicates a σ bond or a triple-bond and $\varepsilon = 1$ indicates a double bond (π -bond). Finally, the density of potential energy ($V(r)$) its related with the Laplacian of density (in atomic units) by the virial theory in the Eq. 8, in which $G(r)$ is the density of kinetic energy.[84-86]

$$\frac{\hbar^2}{4m} \nabla^2\rho(r) = 2G(r) + V(r) \quad (\text{Eq. 8})$$

It was observed that all structures **1-3** containing extensive hydrogen bonding network by AIM analysis (in gas phase or with solvent model SMD). These interactions were primarily characterized by the presence of Bond Paths (BPs) connecting the atoms involved in the non-covalent interactions followed by analysis of AIM data (Table 4). Moreover, the data of optimized structures in gas phase are summarized in the supplementary material (Tables S5 and S6).

The molecular graphs of optimized structures **1-3** are presented in the Figures 8, 9 and 10 and the respective AIM data can be seen in the Table 4. Further, the AIM data of some other highlighted bonds of optimized structures **1-3** (in gas phase or with SMD/DFT) is arranged in the Tables S5 and S6. The non-covalent interactions were mainly characterized by their positive $\nabla^2\rho$ values which indicates a non-covalent interaction and its strengthening trend was determined comparing values of electronic density (ρ) (higher values indicate stronger interactions), ellipticity (ϵ) value closer to zero indicates more directional interactions and density of potential energy (V) with negative values indicate greater electron stability in the interaction.

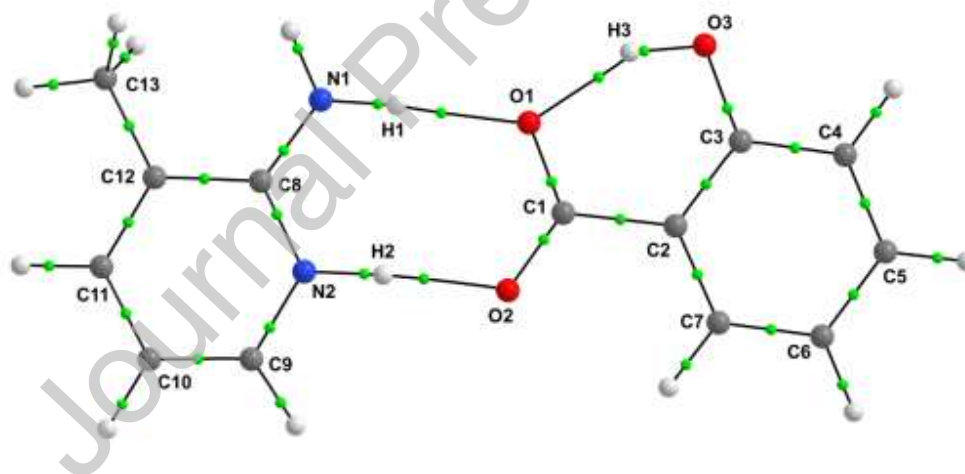


Figure 8 Molecular graph of AIM analysis of optimized structure **1** (with SMD/DFT method). BCPs (green spheres) and BPs (solid and black lines).

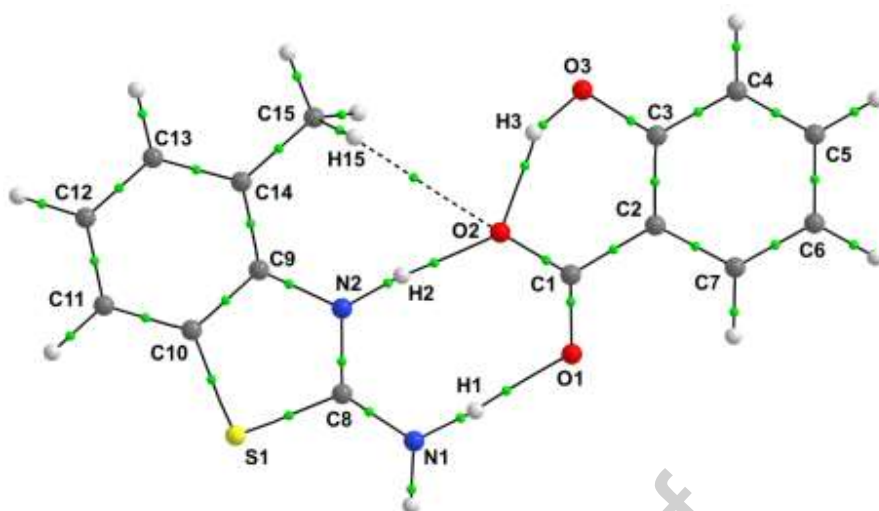


Figure 9 Molecular graph of AIM analysis of optimized structure **2** (with SMD/DFT method). BCPs (green spheres) and BPs (solid and black lines).

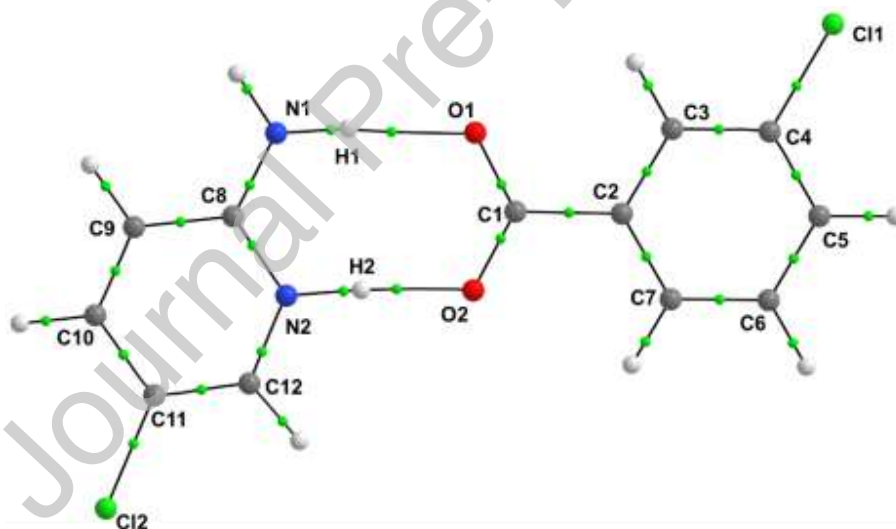


Figure 10 Molecular graph of AIM analysis of optimized structure **3** (with SMD/DFT method). BCPs (green spheres) and BPs (solid and black lines).

Table 4. AIM data of highlighted bonds and non-covalent interactions of optimized structures **1-3** with SMD/DFT method. Electronic density (ρ), Laplacian of density ($\nabla^2\rho$), ellipticity (ϵ) and density of potential energy (V).

Structures	Bond	ρ (e/a^3)	$\nabla^2\rho$ (e/a^5)	ϵ	V (hartree. e/a^3)
------------	------	--------------------	----------------------------	------------	-------------------------

1	O1–H1	0.0350	+0.1137	0.0615	-0.0289
	O2–H2	0.0494	+0.1326	0.0415	-0.0459
	O1–H3	0.0569	+0.1512	0.0331	-0.0579
	O1–C1	0.3553	-0.4887	0.0293	-0.9977
	O2–C1	0.3703	-0.4359	0.0364	-1.0824
2	O1–H1	0.0448	+0.1282	0.0453	-0.0403
	O2–H2	0.0511	+0.1364	0.0457	-0.0485
	O2–H3	0.0556	+0.1515	0.0360	-0.0565
	O2–H15	0.0054	+0.0216	1.3263	-0.0033
	O1–C1	0.3737	-0.4241	0.0390	-1.1015
	O2–C1	0.3512	-0.4916	0.0250	-0.9774
3	O1–H1	0.0362	+0.1140	0.0522	-0.0299
	O2–H2	0.0606	+0.1397	0.0376	-0.0603
	O1–C1	0.3717	-0.4310	0.0367	-1.0906
	O2–C1	0.3625	-0.4538	0.0289	-1.0402

The H-bonds in optimized structures (**1-3**) were verified between O1 or O2 atoms of carboxylic groups (SA⁻ for **1** and **2** and 3CBA⁻ for **3**) and H1–N1- or H2–N2- of their respective molecular cations (2A3MP, 2A4MBT or 2A5CP), as shown in the Figures 8-10. However, for the structure **3**, optimized in gas phase (Figure S.3), was verified a H-bond between N2 and H2–O2- bond, instead O2 and H2–N2-, thus the structure **3** (optimized in gas phase) proved a co-crystal not a molecular salt. Demonstrating the importance of solvent model use for the molecular salt calculations because, in this case, it led to results closer to the experimental data.

Comparing the strength of H-bonds for structures **1-3** through AIM analysis (Table 4) it was verified that the H-bond N2–H2···O2 ($\rho = 0.0494, 0.0511$ and 0.0606 for **1-3**, respectively) is stronger than N1–H1···O1 ($\rho = 0.0350, 0.0448$ and 0.0362 for **1-3**, respectively). The strength of the same H-bonds among the structures **1-3** was observed as $2 > 3 \approx 1$ for N1–H1···O1 and $3 > 2 \approx 1$ for N2–H2···O2. Therefore, for both cases the structure **1** has the weakest H-bonds in the series. To evaluate this behaviour the bond N2–H2 of molecular cations of structures **1** and **2** (2A3MP⁺

and 2A4MBT⁺, respectively) was verified that the bond N2-H2 of 2A3MP⁺ ($\rho = 0.3344$) is stronger than N2-H2 of 2AMB⁺ ($\rho = 0.3305$) which agrees with the expected for 2A3MP that has a higher pKa than 2A4MBT (Table S7). The optimized molecular graphs of AIM analysis of molecular ions 2A3MP⁺, 2A4MBT⁺, 2A5CP⁺, SA⁻_1 (SA⁻ of structure 1), SA⁻_2 (SA⁻ of structure 2) and 3CBA⁻ optimized with SMD/DFT is arranged in the Figure S.4. The molecular graphs of molecular ions optimized with DFT in gas phase were not showed because in very similar, but their AIM data is arranged in the Table S7.

Further, the nature of O-C1 bonds for structures **1-3** was evaluated thus, highest ρ and ε proved that O-C1 bonds have higher π -character than other bonds. It was verified that the O2-C1 bond in structure **1** bears higher value of electronic density ($\rho = 0.3703$) and ellipticity ($\varepsilon = 0.0364$) values than O1-C1 bond ($\rho = 0.3553$ and $\varepsilon = 0.0293$) in the same molecule. For structure **1** the O2-C1 bond has highest π -bond characters, hence the negative charge of carboxylic group is more localized on O1 atom, as discussed in experimental results. Therefore, the H-bonds between molecular ion pairs of structure **1** was established through C1–O1 \cdots H1–N1H1B, a non-usual interaction as discussed in Experimental Section. Moreover, it was observed that O1-C1 bond in compound **2** and **3** bear higher electronic densities, $\rho = 0.3737$ and 0.3717 , respectively and their ellipticity values were found as $\varepsilon = 0.0390$ and 0.0367 , respectively. However, O2-C1 bond in compound **2** and **3** contains electronic densities $\rho = 0.3512$ and 0.3625 with $\varepsilon = 0.0250$ and 0.0289 , respectively. The above-mentioned findings provide enough insights that the O1-C1 bond of structures **2** and **3** has the highest π -bond characters, as the negative charge of carboxylic group is relatively more localized at O2 atom. Thus, the H-bonds between molecular ion pairs of structures **2** and **3** were established through C1=O1 \cdots H1–N1H1B and C1–O2 \cdots H2–⁺N2 interactions in agreement with experimental results. Furthermore, the NBO charge (Table 5) and Wiberg bond index analysis (Table 7) also demonstrate the same tendency. These analyses for other highlighted bonds, H-bonds and the atoms involved in these interactions with optimized with SMD/DFT or gas phase is described in supplementary material (Tables S9 and S10).

Table 5. NBO charges of O1 and O2 atoms of structures **1-3** optimized with SMD/DFT.

NBO charges			
Bonds	1	2	3

O1	-0.813	-0.776	-0.790
O2	-0.784	-0.811	-0.796

Both more negative charged O atoms of structures **1** and **2** (O1 or O2 respectively) has neighbored by an O3-H3 bond which interacts through an intramolecular H-bond O1...H3-O3 ($\rho = 0.0569$) or O2...H3-O3 ($\rho = 0.0556$) for structures **1** and **2**, respectively. It was verified that H-bond O1...H3-O3 of structure **1** is slightly stronger than analogous interaction O2...H3-O3 of structure **2**. This behaviour agrees with experimental observations. Comparing the strength of H-bonds O(1 or 2)...H3-O3 and O2...H2-N2 among structures **1** and **2**, was observed through AIM analysis (Table 4 above) that the O(1 or 2)...H3-O3 interaction is slightly stronger than O2...H2-N2. This behaviour can be explained by the distance between H...A atoms, that is short for O(1 or 2)...H3-O3 than O2...H2-N2 for both structures (experimentally and theoretically as can be seen in Table S3 and S4).

However, through NBO (Table 6) and Wiberg bond index analysis (Table 7) was observed an inverse behaviour of strength (but again with slight differences). It was verified that the O2...H2-N2 is slightly stronger than O(1 or 2)...H3-O3 interaction for both **1** and **2** structures. This inversion of trend can be explained by the bond angle of O2...H2-N2 which is higher than O(1 or 2)...H3-O3 (Table S4) that allows a better orbital alignment to a higher donor-acceptor interaction for O2...H2-N2 (as can be observed in the NBO surfaces plots for these interactions in given in Figures 11 and 12 for O2...H2-N2 beyond Figures S.8 and S.11 for O(1 or 2)...H3-O3). Another data that reinforces this explanation is the analysis of Laplacian of density ($\nabla^2\rho$) from AIM analysis that presented positive values for both interactions, but higher for O(1 or 2)...H3-O3 ($\nabla^2\rho = +0.1512$ and $+0.1515$, for structures **1** and **2**, respectively) than O2...H2-N2 interaction ($\nabla^2\rho = +0.1326$ and $+0.1364$, for structures **1** and **2** respectively), which can indicate an interaction more dispersive for O(1 or 2)...H3-O3 than O2...H2-N2. These non-covalent interactions (O...H3-O3), as discussed in experimental results, contributes to direct the supramolecular structure of their respective molecular salts, especially for structure **1** that will be discussed in molecular salt dimer structures (*vide infra*).

Table 6. Second Order Perturbation Theory Analysis of Fock Matrix in NBO basis of main donor-acceptor interactions of **1-3** optimized with SMD/DFT method.

Structure	Donor	Acceptor	$E^{(2)}$ kcal/mol	$E(j)-E(i)$ a.u.	$F(i,j)$ a.u.
1	$n(1)_{O1}$	σ^*_{N1-H1}	8.85	1.14	0.090
	$n(2)_{O2}$	σ^*_{N2-H2}	25.44	0.69	0.120
	$n(2)_{O1}$	σ^*_{O3-H3}	23.31	0.69	0.115
2	$n(2)_{O1}$	σ^*_{N1-H1}	21.22	0.70	0.110
	$n(2)_{O2}$	σ^*_{N2-H2}	17.14	0.66	0.096
	$n(2)_{O2}$	σ^*_{O3-H3}	16.39	0.69	0.097
3	$n(2)_{O1}$	σ^*_{N1-H1}	14.88	0.70	0.093
	$n(2)_{O2}$	σ^*_{N2-H2}	35.99	0.70	0.143

Delocalization energy ($E^{(2)}$), Energy difference between i (donor) and j (acceptor) NBO orbitals ($E(j)-E(i)$) and Fock matrix element i and j NBO orbital ($F(i,j)$).

Table 7: Wiberg bond index of atoms involved in the main H-bonds between molecular ions of structures **1-3** optimized with SMD/DFT method.

Bond	Wiberg bond index		
	1	2	3
O1–H1	0.055	0.085	0.062
O2–H2	0.099	0.101	0.128
N2–H2	0.655	0.635	0.623
O1–H3	0.096	-	-
O2–H3	-	0.091	-

Meanwhile, the structure **3**, which not exhibit this type of intramolecular interaction, showed a stronger O1⋯H1–N1 interaction than structure **1** but weaker than **2**. The presence of Cl atoms play an important role in the supramolecular **3** arrangement through the non-classical non-covalent interaction i.e., Cl⋯Cl beyond polarizing the electronic density of structure **3** through withdrawal inductive effect (apart from the donor effect by resonance), and this polarization reflects on its chemical reactivity, as demonstrated in the GRD analysis, which in the other hand reflects on its non-covalent interactions. Especially for the O2⋯H2–N2 which is stronger than structures **1** and **2**. This, non-covalent interaction combined with its chemical reactivity must be responsible for the structure **3** is a molecular salt. Moreover, the electronic availability of Cl1 (from acid) and Cl2 (from base) was evaluated though NBO charge (Table S10) analysis which demonstrate that Cl1 presented a negative charge (-0.026) while Cl2 presented a positive charge (0.010). Beyond that, the Cl1 presented a weaker bond with C4 atom (Cl1–C4) than Cl2 with Cl1 atom (Cl2–Cl1). This behaviour was verified by AIM analysis (Table S6) through which it was verified a $\rho = 0.1862$ for Cl1–C4 and $\rho = 0.1937$ for Cl2–Cl1) and by Wiberg index analysis (Table S9) through which it was verified a bond index 1.036 for Cl1–C4 and 1.050 for Cl2–Cl1. Thus, the weaker bond Cl1–C4 than Cl2–Cl1 combined with the negative charge of Cl1 against the positive charge of Cl2 demonstrated that Cl1 atom from acid is able to interact through secondary interactions while that Cl2 from base was found inert to this type of interaction. These observations corroborate the experimental results which demonstrated that just Cl1 from acid interacts though secondary interactions while Cl2 was not present in the non-covalent

interactions in extended structures. The DFT calculations (in gas phase) demonstrate the same trend observed with SMD/DFT for AIM analysis, but inverse with Wiberg analysis beyond the both Cl atoms showed positive charge. Demonstrating again the importance of solvent model use for these molecular salts calculation.

These observed trends for H-bonding among the structures **1-3** ($2 > 3 \approx 1$ for N1-H1...O1 and $3 > 2 \approx 1$ for N2-H2...O2) thought AIM analysis were also observed by NBO analysis. Thus, the NBO analysis showed (generally) higher delocalization energies ($E^{(2)}$) for the stronger H-bonds of structures **1-3**. The verified trends of NBO delocalization energies (donor-acceptor) were $2 > 3 > 1$ for N1-H1...O1 and $3 > 1 > 2$ for N2-H2...O2 (Tables 6 and S8). The NBO surfaces plot of orbitals involved in the more energetic donor-acceptor interactions of H-bonds of structures **1-3** are shown in the Figures 11, 12 and 13. The plots of other NBO surfaces are given in the supplementary material (Figures S.5-S.15).

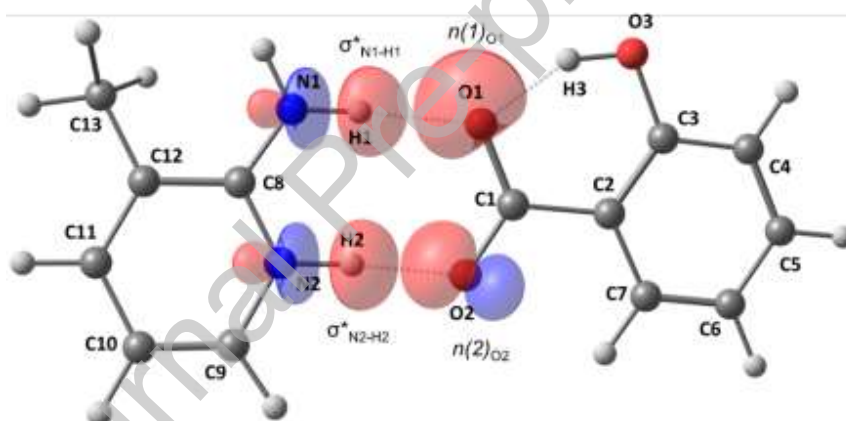


Figure 11. NBO surfaces plot of structure **1** optimized with SMD/DFT method. Non-bonding orbitals $n(1)_{O1}$ and $n(2)_{O2}$ which interact with anti-bonding orbitals σ^*_{N1-H1} and σ^*_{N2-H2} .

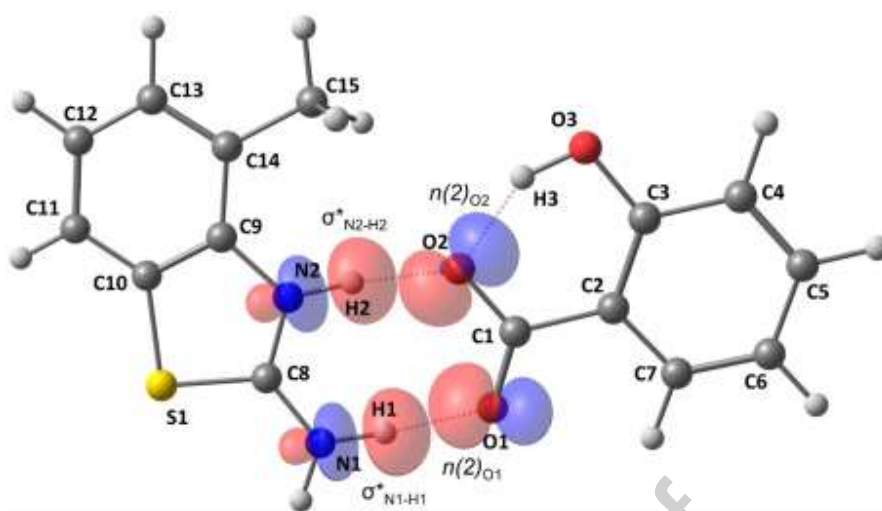


Figure 12. NBO surfaces plot of structure **2** optimized with SMD/DFT method. Non-bonding orbitals $n(2)_{O1}$ and $n(2)_{O2}$ which interact with anti-bonding orbitals σ^*_{N1-H1} and σ^*_{N2-H2} .

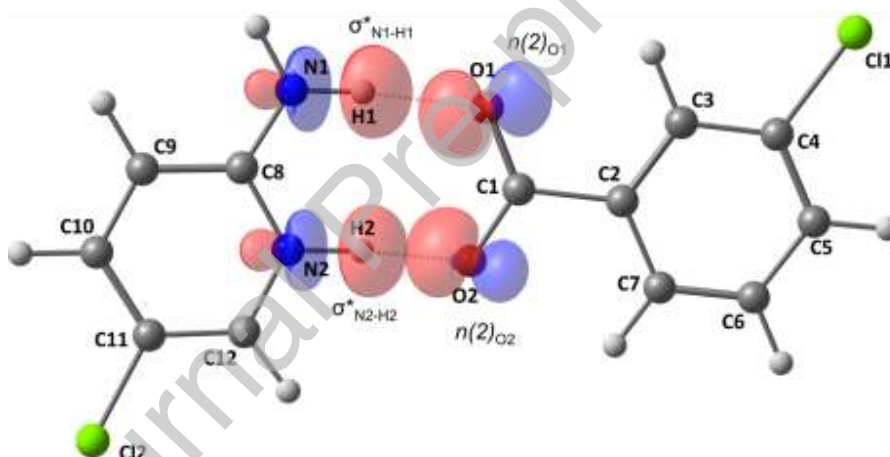


Figure 13. NBO surfaces plot of structure **3** optimized with SMD/DFT method. Non-bonding orbitals $n(2)_{O1}$ and $n(2)_{O2}$ which interact with anti-bonding orbitals σ^*_{N1-H1} and σ^*_{N2-H2} .

It was observed that the N2-H2...O2 bond of structure **1** the most important delocalization energy ($n(2)_{O2} \rightarrow \sigma^*_{N2-H2}$) of this H-bond has higher $E^{(2)}$ (25.44 kcal/mol) than **2** (17.14 kcal/mol), indicating a stronger H-bond for **1** than **2**. However it is important emphasized that for structure **2** the interaction $n(1)_{O2} \rightarrow \sigma^*_{N2-H2}$ has higher $E^{(2)}$ (15.13 kcal/mol) than **1** (6.69 kcal/mol), in the same direction of AIM analysis (Table S8). Wiberg bond index analysis was performed to further investigate these H-bonds and this analysis revealed that trends of H-bonds strength were observed equivalent to AIM analysis: $2 > 3 > 1$ for N1-H1...O1 and $3 > 2 \approx 1$ for N2-H2...O2 (Table

7). Besides that, the O1-H3...O3 of structure **1** proved stronger than O2-H3...O3 of structure **2** by Wiberg bond index. Moreover, other Wiberg bond index also agrees with another bond strength trends as verified by AIM analysis (Table S9).

Thus, through the conjunct examination of these analysis (AIM, NBO and Wiber bond index) was demonstrated that the order of H-bond strength is $2 > 3 > 1$ for N1-H1...O1 and $3 > 2 \approx 1$ for N2-H2...O2. This behaviour, particularly for the strength of N2-H2...O2 bond of structure **2** in relation to **1**, must be related (beyond other chemical reactivity parameters of structures **1** and **2**) with the presence of fused heterocyclic ring with a S heteroatom in the structure **2** which presented donor-acceptor interactions between bonding and anti-bonding orbitals of S1-C8 bond and N1-H1 and N2-H2 bonds (Table S8 and Figures S.12-S.14) that can weakening the N1-H1 and N2-H2 bonds (by increasing the population of the respective anti-bonding N1-H1 and N2-H2 orbitals) which can strengthen the respective H-bonds N1-H1...O1 and N2-H2...O2, that can explain the strength verified for these H-bonds in structure **2**.

Finally, after studying the molecular salts formation, their reactivity and the nature of bond and non-covalent interactions which contribute towards its formation, we analyzed the non-covalent interactions for experimental geometry of crystals. That is, we performed single point calculations with B3LYP-D3/6-311+G(d,p) method of structures **1-3** and of their respective dimers (that is, two pairs of molecular salts, **1-1***, **2-2*** and **3-3***) **1-D**, **1-D2**, **2-D** and **3D**, respectively. Beyond that, the molecular salt **1** has another alternative way to interact with each other (**1-1'**), thus with a different arrangement of their structure that we called **1-D2**, which was also analyzed. All these structures were cut-off from their crystallographic information file. The analysis of dimers with their experimental geometries aims to investigate the architecture of non-covalent interactions that leads to the adopted arrangement of molecular salt in its crystalline structure.

The AIM data for structures **1-3** calculated with single point calculations with DFT in gas phase from their experimental geometries is arranged in the Table S11. Overall, there was a weakening of non-covalent interactions and a strengthening of covalent bonds in relation to optimized structures in gas phase and with SMD/SMD (Tables S5 and S6), although the AIM data for optimized structures **1-3** with SMD/DFT showed a behaviour of bonds and non-covalent bonds strength closer to structures with experimental geometry. However, the trend of H-bond

strength for structures **1-3** calculated from their experimental geometries is $3 > 2 > 1$ for O1...H1-N1 (with $\rho = 0.0377$, 0.0288 and 0.0217 for structures **3**, **2** and **1**, respectively). Moreover trend is found to be $3 > 1 > 2$ for O2...H2-N2 (with $\rho=0.0502$, 0.0334 and 0.0318 , for structures **3**, **1** and **2**, respectively) that is different tendencies than verified for optimized structures with SMD/DFT.

As for optimized structures, in agreement with experimental results, AIM analysis from single point calculations showed that the O2-C1 bond ($\rho=0.3787$, $\varepsilon=0.0408$) has larger π -character (presenting larger ρ , $\nabla^2\rho$, ε and V , which indicate larger π -character) than O1-C1 bond ($\rho=0.3619$, $\varepsilon=0.0346$) for structure **1** (Table S11). Beyond that the O1-C1 bond ($\rho=0.3827$, $\varepsilon=0.0445$ and $\rho=0.3865$, $\varepsilon=0.0394$, respectively) of structures **2** and **3** (Table S11) has larger π -character (presenting larger ρ , $\nabla^2\rho$, ε and V) than O2-C1 bond ($\rho=0.3673$, $\varepsilon=0.0248$ and $\rho=0.3620$, $\varepsilon=0.0342$, respectively). Thus, the H-bonds for structure **1** was established *via* C-O...H-NH and C=O...H⁺N interactions and for structures **2** and **3** the H-bonds between molecular ions was established *via* C=O...H-NH and C-O...H⁻N interactions as discussed in experimental and optimized structures results.

The observed trends of H-bonds strength among the structures **1-3** from single point calculations (with experimental geometry) were also observed by NBO analysis (Table S12). It was also noticed that a general decrease of delocalization energies of donor-acceptor interactions occurs. This behaviour was also observed comparing the NBO analysis with SMD/DFT in relation to gas phase.

Moreover, the AIM properties of structures **1-3** dimers, **1-D**, **1-D2**, **2-D** and **3D** demonstrate the presence of several non-covalent interactions between the molecular ions, which is expected for a crystal structure (Figures 14-17, Tables S13-S18, Figures S16-S19). Although the presence of non-classical interactions beyond the classical has been highlighted due its influence in the arrangement of the salts in the respective crystal structure arrangement. Because of the several tags of atoms number in the Figures S16-S19 (that has the labelling of dimers **1-D**, **1-D2**, **2-D** and **3-D**) difficult the analysis of intermolecular non-covalent interactions the Figures 14-17 has their labelling scheme cleaned and that has just labels for BCPs of non-covalent interactions. Their respective AIM data is shown in the Tables S15-S18. Meanwhile, it was observed that these non-covalent interactions between molecular salts delocalize the electronic density of molecules which leads to a slight weakening of H-bonds between molecular ions

(Tables S11 and S13). The weakening of non-covalent interactions between molecular ions of **1-D**, **2-D** and **3-D** in relation to their respective molecular salts **1-3** can also be related to the arrangement of these interactions as confirmed by AIM data.

The strength tendencies of H-bonds established between molecular ions of **1-D**, **2-D** and **3-D** were the same as for structures the respective salts **1-3** from single point calculations. The **3-D** showed stronger H-bonds O1...H1-N1 ($\rho=0.0376$) than **2-D** and **1-D** ($\rho=0.0282$, $\rho=0.0213$, respectively) beyond stronger O2...H2-N2 bond ($\rho=0.0499$) than **1-D** and **2-D** ($\rho=0.0330$, $\rho=0.0311$, respectively).

Moreover, as mentioned above, the presence of intramolecular H-bonds O1...H3-O3 or O2...H3-O3 in the molecular salts **1** and **2** proved to be important to their supramolecular structure, particularly for structure **1**. Analysing the different supramolecular arrangement **1-D2**, (Figure 15), it was found that a non-covalent interaction **f** (O3*-H1b*) with $\rho=0.0136$ (Table S16) which collaborates to guide the supramolecular arrangement of molecular salt **1**, as discussed in experimental results. Moreover, O3 also interacts through non-covalent interactions **e** (O3*-H13b*) with $\rho=0.0052$ and **k** (O3*-C9*) with $\rho=0.0056$ (Table S16) which also influences in the adopted structure of the molecular salt **1** crystal.

Further, the secondary non-covalent interactions between dimers of the compounds have been verified *via* non-classical secondary interactions such O...O and H...H (**1-D**), O...S (**2-D**), and Cl...Cl (**3-D**) besides π -stacking, C...H-C and other interactions. Such secondary interactions engineer the supramolecular arrangements of molecular salts to their respective organic crystal structures. Although very important, these interactions are considerably weaker than H-bonds showing electronic density (ρ) with values ranging around 0.006 and 0.001 (Tables S15-S18) against ρ values ranging around 0.10 and 0.04 for H-bonding (Tables 4, S5, S11 and S13). In general, the molecular salt **1** showed stronger secondary non-covalent interactions than **2** followed by **3**; however, the molecular salt **3** showed the stronger H-bonds between molecular ions than molecular salts **1** and **2**.

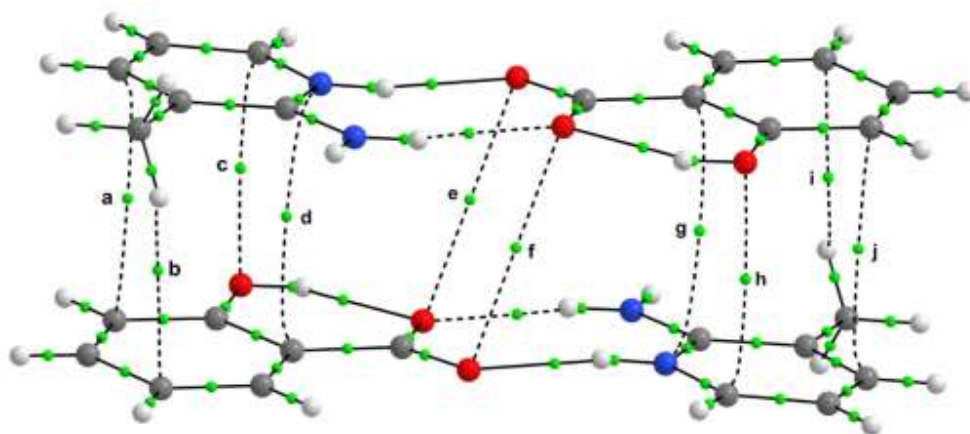


Figure 14. Molecular graphs of AIM analysis of structure **1** dimer (**1-D**) calculated with DFT in gas phase (single point). BCPs (green spheres) and BPs (solid and dashed black lines).

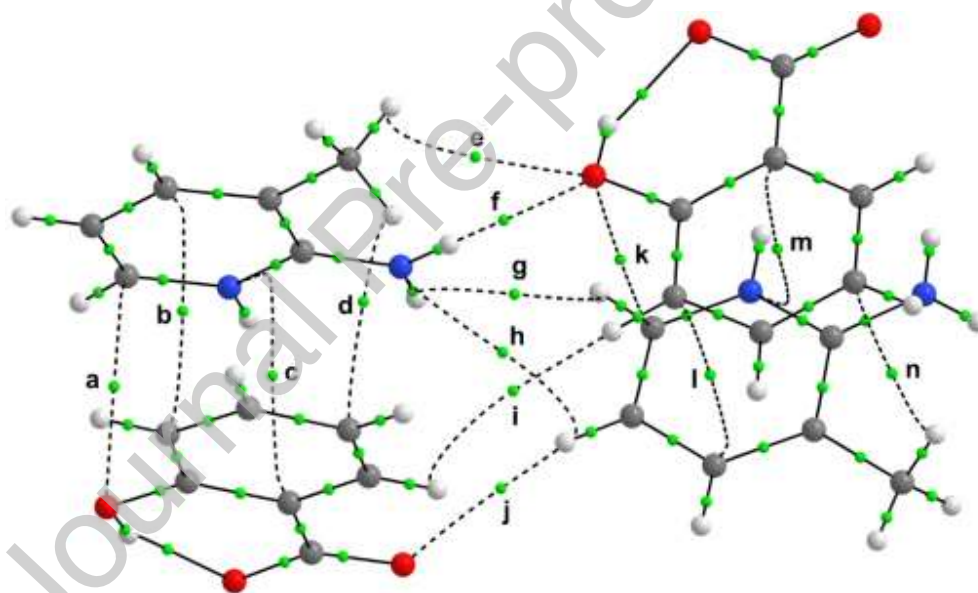


Figure 15. Molecular graphs of AIM analysis of structure **1** dimer in a different arrangement (**1-D2**) calculated with DFT in gas phase (single point). BCPs (green spheres) and BPs (solid and dashed black lines).

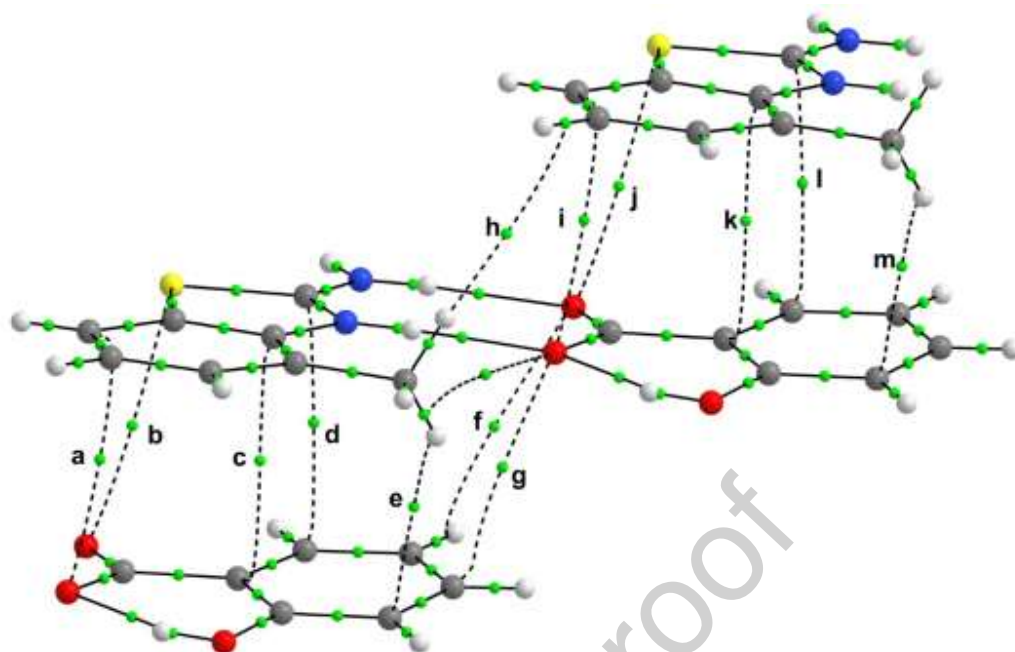


Figure 16. Molecular graphs of AIM analysis of structure **2** dimer (**2-D**) calculated with DFT in gas phase (single point). BCPs (green spheres) and BPs (solid and dashed black lines).

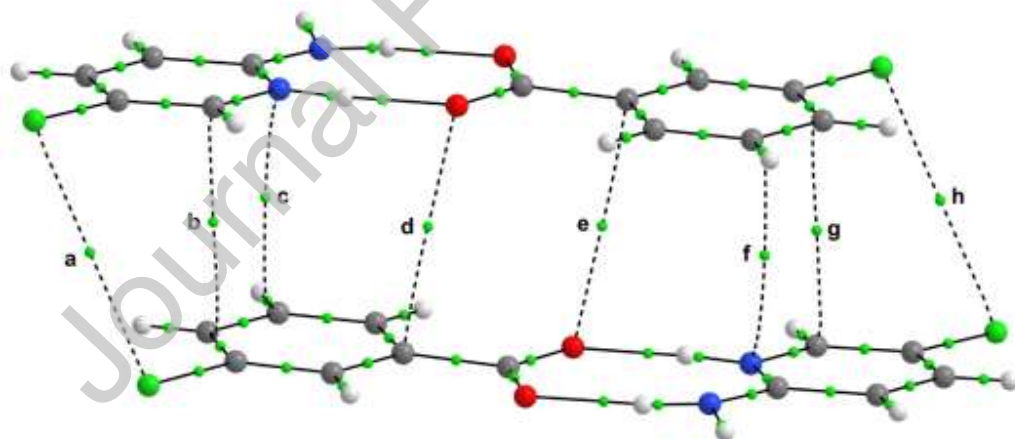


Figure 17 Molecular graphs of AIM analysis of structure **3** dimer (**3-D**) calculated with DFT in gas phase (single point). BCPs (green spheres) and BPs (solid and dashed black lines).

Overall, the use of solvent model SMD presented a better description of experimental observations for structures **1-3**.

Conclusion

Three molecular salts of general representations BA, were obtained where acid and base reacted in a 1:1 molar ratio. Acid was protonated and endocyclic N of the respective base was found to accept the proton. Molecular salts are stabilized by conventional H-bonding and charge assisted interaction. The Cl function in acid was found more polar which was capable to interact with oxygen atom of neighbouring carboxylic function, while Cl function of the base in AB pair of compound **3**, was inactive in this respect and was not a part of non-covalent interactions in extended structures. All reactions are straightforward and crystals were obtained as a result of slow evaporation. Acid/Base fragments in all three molecular salts were coplanar with negligible deviation. Secondary interactions in all molecular salts have been evaluated theoretically and were found to be in close agreement with experimental observations. The AIM analysis of secondary non-covalent interactions such O \cdots O and H \cdots H, O \cdots S, Cl \cdots Cl, beyond π -stacking, C \cdots H-C and other interactions demonstrates that these interactions collaborate stabilize the salts in its molecular arrangements. Thus, these non-covalent interactions proved important to direct the supramolecular arrangements of molecular salts. Moreover, FMO, GRD, AIM, NBO, NBO charge and Wiberg bond index analyses showed a stronger stability of entitled compounds due to strength of non-covalent interactions. Thus, theoretical analysis is a good alternative tool to study the possibility of molecular salts formation *via* analysing their non-covalent interactions.

Acknowledgement

We are thankful to University of Malakand for financial support.

Conflict of interest

Authors have no conflict of interest to be declared

CCDC Reference

CCDC No. 1981714, 1981715 and 1981716 contain the supplementary crystallographic data for molecular salts **1-3**. These data can be obtained free of charge via <http://www.ccdc.cam.ac.uk/conts/retrieving.html>, or from the Cambridge Crystallographic Data Centre, 12 Union Road, Cambridge CB2 1EZ, UK; fax: (+44) 1223-336-033; or e-mail: deposit@ccdc.cam.ac.uk.

References

- [1] C. Janiak, A critical account on π - π stacking in metal complexes with aromatic nitrogen-containing ligands, *Journal of the Chemical Society, Dalton Transactions*, (2000) 3885-3896.
- [2] G.R. Desiraju, C-H \cdots O and other weak hydrogen bonds. From crystal engineering to virtual screening, *Chemical Communications*, (2005) 2995-3001.
- [3] L. Wang, R.A. Friesner, B. Berne, Competition of electrostatic and hydrophobic interactions between small hydrophobes and model enclosures, *The Journal of Physical Chemistry B*, 114 (2010) 7294-7301.
- [4] P.A. Wood, F.H. Allen, E. Pidcock, Hydrogen-bond directionality at the donor H atom—analysis of interaction energies and database statistics, *CrystEngComm*, 11 (2009) 1563-1571.
- [5] G.R. Desiraju, Reflections on the hydrogen bond in crystal engineering, *Crystal Growth & Design*, 11 (2011) 896-898.
- [6] Ö. Almarsson, M.J. Zaworotko, Crystal engineering of the composition of pharmaceutical phases. Do pharmaceutical co-crystals represent a new path to improved medicines?, *Chemical communications*, (2004) 1889-1896.
- [7] S.L. Childs, L.J. Chyall, J.T. Dunlap, V.N. Smolenskaya, B.C. Stahly, G.P. Stahly, Crystal engineering approach to forming cocrystals of amine hydrochlorides with organic acids. Molecular complexes of fluoxetine hydrochloride with benzoic, succinic, and fumaric acids, *Journal of the American Chemical Society*, 126 (2004) 13335-13342.
- [8] J.C. MacDonald, G.M. Whitesides, Solid-state structures of hydrogen-bonded tapes based on cyclic secondary diamides, *Chemical Reviews*, 94 (1994) 2383-2420.

- [9] Z. Mu, L. Shu, H. Fuchs, M. Mayor, L. Chi, Two dimensional chiral networks emerging from the Aryl- F \cdots H hydrogen-bond-driven self-assembly of partially fluorinated rigid molecular structures, *Journal of the American Chemical Society*, 130 (2008) 10840-10841.
- [10] G.R. Desiraju, A bond by any other name, *Angewandte Chemie International Edition*, 50 (2011) 52-59.
- [11] J. Yao, J.-M. Chen, Y.-B. Xu, T.-B. Lu, Enhancing the solubility of 6-mercaptopurine by formation of ionic cocrystal with zinc trifluoromethanesulfonate: single-crystal-to-single-crystal transformation, *Crystal growth & design*, 14 (2014) 5019-5025.
- [12] J.-M. Chen, S. Li, T.-B. Lu, Pharmaceutical cocrystals of ribavirin with reduced release rates, *Crystal growth & design*, 14 (2014) 6399-6408.
- [13] Z.-Z. Wang, J.-M. Chen, T.-B. Lu, Enhancing the hygroscopic stability of S-oxiracetam via pharmaceutical cocrystals, *Crystal growth & design*, 12 (2012) 4562-4566.
- [14] P.L. Gould, Salt selection for basic drugs, *International Journal of Pharmaceutics*, 33 (1986) 201-217.
- [15] N. Geng, J.-M. Chen, Z.-J. Li, L. Jiang, T.-B. Lu, Approach of cocrystallization to improve the solubility and photostability of tranilast, *Crystal growth & design*, 13 (2013) 3546-3553.
- [16] Y. Chi, W. Xu, Y. Yang, Z. Yang, H. Lv, S. Yang, Z. Lin, J. Li, J. Gu, C.L. Hill, Three candesartan salts with enhanced oral bioavailability, *Crystal Growth & Design*, 15 (2015) 3707-3714.
- [17] G.A. Jeffrey, G.A. Jeffrey, *An introduction to hydrogen bonding*, Oxford university press New York 1997.
- [18] G.R. Desiraju, Hydrogen bridges in crystal engineering: interactions without borders, *Accounts of chemical research*, 35 (2002) 565-573.
- [19] G.P. Stahly, Diversity in single-and multiple-component crystals. The search for and prevalence of polymorphs and cocrystals, *Crystal growth & design*, 7 (2007) 1007-1026.
- [20] D. Lide, H. Fredrikse, *CRC handbook of chemistry and physics*. CRC Press, Boca Raton, FL, *CRC handbook of chemistry and physics*. 75th ed. CRC Press, Boca Raton, FL., (1994) -.
- [21] M.K. Stanton, S. Tufekcic, C. Morgan, A. Bak, Drug substance and former structure property relationships in 15 diverse pharmaceutical co-crystals, *Crystal Growth and Design*, 9 (2009) 1344-1352.

- [22] C.B. Aakeröy, M.E. Fasulo, J. Desper, Cocrystal or salt: does it really matter?, *Molecular Pharmaceutics*, 4 (2007) 317-322.
- [23] A.J. Cruz-Cabeza, Acid–base crystalline complexes and the p K a rule, *CrystEngComm*, 14 (2012) 6362-6365.
- [24] A. Delori, P.T. Galek, E. Pidcock, M. Patni, W. Jones, Knowledge-based hydrogen bond prediction and the synthesis of salts and cocrystals of the anti-malarial drug pyrimethamine with various drug and GRAS molecules, *CrystEngComm*, 15 (2013) 2916-2928.
- [25] S.L. Morissette, Ö. Almarsson, M.L. Peterson, J.F. Remenar, M.J. Read, A.V. Lemmo, S. Ellis, M.J. Cima, C.R. Gardner, High-throughput crystallization: polymorphs, salts, co-crystals and solvates of pharmaceutical solids, *Advanced drug delivery reviews*, 56 (2004) 275-300.
- [26] A.T. Serajuddin, Salt formation to improve drug solubility, *Advanced drug delivery reviews*, 59 (2007) 603-616.
- [27] R. Patra, H.M. Titi, I. Goldberg, Crystal engineering of molecular networks: tailoring hydrogen-bonding self-assembly of tin-tetrapyridylporphyrins with multidentate carboxylic acids as axial ligands, *Crystal growth & design*, 13 (2013) 1342-1349.
- [28] L.C. Gilday, S.W. Robinson, T.A. Barendt, M.J. Langton, B.R. Mullaney, P.D. Beer, Halogen bonding in supramolecular chemistry, *Chemical reviews*, 115 (2015) 7118-7195.
- [29] J.C. MacDonald, P.C. Dorrestein, M.M. Pilley, Design of supramolecular layers via self-assembly of imidazole and carboxylic acids, *Crystal Growth & Design*, 1 (2001) 29-38.
- [30] M.L. Highfill, A. Chandrasekaran, D.E. Lynch, D.G. Hamilton, Superstructural variety from an alkylated triazine: Formation of one-dimensional hydrogen-bonded arrays or cyclic rosettes, *Crystal growth & design*, 2 (2002) 15-20.
- [31] P. Vishweshwar, A. Nangia, V.M. Lynch, Recurrence of carboxylic acid– pyridine supramolecular synthon in the crystal structures of some pyrazinecarboxylic acids, *The Journal of organic chemistry*, 67 (2002) 556-565.
- [32] G.S. Nichol, W. Clegg, Classical and weak hydrogen bonding interactions between 4, 4'-bipyridine and organic acids: from co-crystal to organic complex, *Crystal Growth and Design*, 9 (2009) 1844-1850.

- [33] Y.-B. Men, J. Sun, Z.-T. Huang, Q.-Y. Zheng, Organic hydrogen-bonded interpenetrating diamondoid frameworks from modular self-assembly of methanetetra benzoic acid with linkers, *CrystEngComm*, 11 (2009) 978-979.
- [34] V. Sethuraman, N. Stanley, P.T. Muthiah, W. Sheldrick, M. Winter, P. Luger, M. Weber, Isomorphism and Crystal Engineering: Organic ionic ladders formed by supramolecular motifs in pyrimethamine salts, *Crystal growth & design*, 3 (2003) 823-828.
- [35] N. Stanley, V. Sethuraman, P.T. Muthiah, P. Luger, M. Weber, Crystal engineering of organic salts: Hydrogen-bonded supramolecular motifs in pyrimethamine hydrogen glutarate and pyrimethamine formate, *Crystal growth & design*, 2 (2002) 631-635.
- [36] N. Stanley, P. Muthiah, S. Geib, P. Luger, M. Weber, M. Messerschmidt, The novel hydrogen bonding motifs and supramolecular patterns in 2, 4-diaminopyrimidine–nitrobenzoate complexes, *Tetrahedron*, 61 (2005) 7201-7210.
- [37] E. Khan, A. Khan, Z. Gul, F. Ullah, M.N. Tahir, M. Khalid, H.M. Asif, S. Asim, A.A.C. Braga, Molecular salts of terephthalic acids with 2-aminopyridine and 2-aminothiazole derivatives as potential antioxidant agents: Base-Acid-Base type architectures, *Journal of Molecular Structure*, 1200 (2020) 127126.
- [38] K. Sepčić, Bioactive alky pyridinium compounds from marine sponges, *Journal of Toxicology: Toxin Reviews*, 19 (2000) 139-160.
- [39] K. Thanigaimani, N.C. Khalib, A. Farhadikoutenaie, S. Arshad, I.A. Razak, Synthesis and Structural Characterization of Two New Charge-Assisted Hydrogen-Bonded Supramolecular Networks in 2-Amino-4-methylpyridinium Isophthalate Dihydrate and 2-Amino-5-methylpyridinium Hydrogen Isophthalate, *Molecular Crystals and Liquid Crystals*, 606 (2015) 246-261.
- [40] S. Saha, M.K. Mishra, C.M. Reddy, G.R. Desiraju, From molecules to interactions to crystal engineering: mechanical properties of organic solids, *Accounts of chemical research*, 51 (2018) 2957-2967.
- [41] D.E. Lynch, G.D. Jones, Geometry of the 2-aminoheterocyclic–carboxylic acid R22 (8) graph set: implications for crystal engineering, *Acta Crystallographica Section B: Structural Science*, 60 (2004) 748-754.

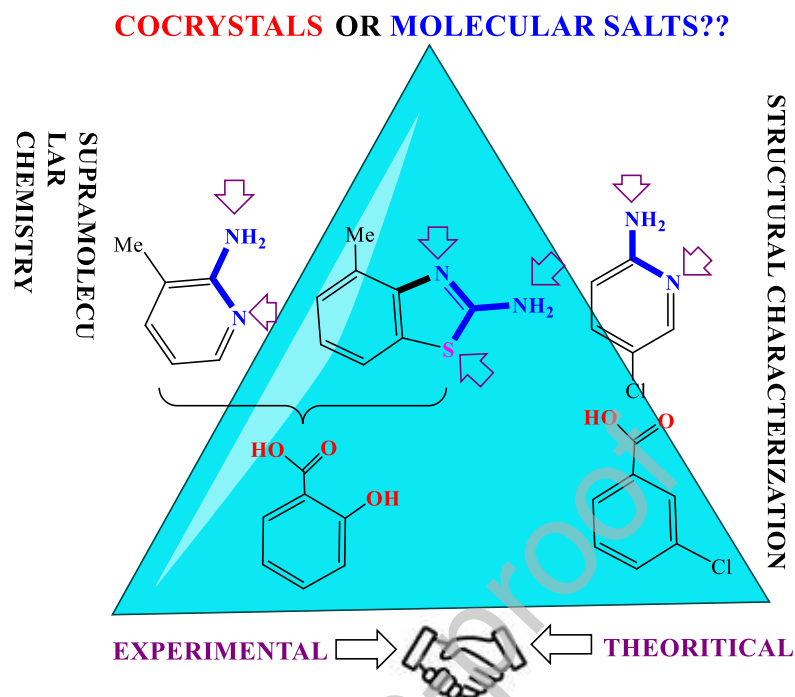
- [42] E. Khan, M. Khalid, Z. Gul, A. Shahzad, M.N. Tahir, H.M. Asif, S. Asim, A.A.C. Braga, Molecular structure of 1, 4-bis (substituted-carbonyl) benzene: A combined experimental and theoretical approach, *Journal of Molecular Structure*, (2019) 127633.
- [43] A. Altomare, M.C. Burla, M. Camalli, G.L. Casciarano, C. Giacovazzo, A. Guagliardi, A.G. Moliterni, G. Polidori, R. Spagna, SIR97: a new tool for crystal structure determination and refinement, *Journal of Applied Crystallography*, 32 (1999) 115-119.
- [44] G. Sheldrick, New features added to the refinement program SHELXL since 2008 are described and explained, *Acta Crystallographica C*, 71 (2015) 3-8.
- [45] L.J. Farrugia, WinGX suite for small-molecule single-crystal crystallography, *Journal of Applied Crystallography*, 32 (1999) 837-838.
- [46] A.L. Spek, Structure validation in chemical crystallography, *Acta Crystallographica Section D: Biological Crystallography*, 65 (2009) 148-155.
- [47] M. Frisch, G. Trucks, H. Schlegel, G. Scuseria, M. Robb, J. Cheeseman, Gaussian 09, Revision B. 01. Gaussian 09, Revision B. 01. Wallingford CT: Gaussian, Inc, 2009.
- [48] A. Becke, Density-functional thermochemistry. III. The role of exact exchange (1993) *J. Chem. Phys.*, 98 5648.
- [49] C. Lee, W. Yang, R.G. Parr, Development of the Colle-Salvetti correlation-energy formula into a functional of the electron density, *Physical review B*, 37 (1988) 785.
- [50] S. Grimme, J. Antony, S. Ehrlich, H. Krieg, A consistent and accurate ab initio parametrization of density functional dispersion correction (DFT-D) for the 94 elements H-Pu, *The Journal of chemical physics*, 132 (2010) 154104.
- [51] R. Ditchfield, W.J. Hehre, J.A. Pople, Self-consistent molecular-orbital methods. IX. An extended Gaussian-type basis for molecular-orbital studies of organic molecules, *The Journal of Chemical Physics*, 54 (1971) 724-728.
- [52] W.J. Hehre, R. Ditchfield, J.A. Pople, Self-consistent molecular orbital methods. XII. Further extensions of Gaussian-type basis sets for use in molecular orbital studies of organic molecules, *The Journal of Chemical Physics*, 56 (1972) 2257-2261.
- [53] V.A. Rassolov, J.A. Pople, M.A. Ratner, T.L. Windus, 6-31G* basis set for atoms K through Zn, *The Journal of chemical physics*, 109 (1998) 1223-1229.
- [54] R.F. Bader, A quantum theory of molecular structure and its applications, *Chemical Reviews*, 91 (1991) 893-928.

- [55] R. Bader, *Atoms in Molecules. A Quantum Theory*, International Series of Monographs on Chemistry Clarendon Press, Oxford, 1994.
- [56] F. Weinhold, C.R. Landis, Natural bond orbitals and extensions of localized bonding concepts, *Chemistry Education Research and Practice*, 2 (2001) 91-104.
- [57] T. Keith, AIMAll (Version 16.05. 18); TK Gristmill Software: Overland Park, KS, 2016, Available at: aim.tkgristmill.com.
- [58] G.A. Andrienko, *Chemcraft. Graphical Software for Visualization of Quantum Chemistry Computations*, 2010.
- [59] E. Khan, T. Ahmad, Z. Gul, F. Ullah, M.N. Tahir, A. Noor, Methyl-substituted 2-aminothiazole--based cobalt (II) and silver (I) complexes: synthesis, X-ray structures, and biological activities, *Turkish Journal of Chemistry*, 43 (2019) 857-868.
- [60] E. Khan, Z. Gul, A. Shahzad, M.S. Jan, F. Ullah, M. Tahir, A. Noor, Coordination compounds of 4, 5, 6, 7-tetrahydro-1 H-indazole with Cu (II), Co (II) and Ag (I): structural, antimicrobial, antioxidant and enzyme inhibition studies, *Journal of Coordination Chemistry*, 70 (2017) 4054-4069.
- [61] S.A. Khan, A. Noor, R. Kempe, H. Subhan, A. Shah, E. Khan, Syntheses, molecular structure, and electrochemical investigations of cobalt (II), copper (II), palladium (II), and zinc (II) complexes with 3-methylpyrazole, *Journal of Coordination Chemistry*, 67 (2014) 2425-2434.
- [62] E. Khan, A. Shahzad, M.N. Tahir, A. Noor, Antioxidant potential and secondary reactivity of bis $\{ \text{diphenyl (2-pyridyl) phosphino} \}$ copper (II) complex, *Turkish Journal of Chemistry*, 42 (2018) 1299-1309.
- [63] G. Varsanyi, *Vibrational spectra of benzene derivatives*, Elsevier 2012.
- [64] L. Bellamy, *The infra-red spectra of complex molecules*, Springer Science & Business Media 2013.
- [65] X.-h. Guan, G.-h. CHEN, C. Shang, ATR-FTIR and XPS study on the structure of complexes formed upon the adsorption of simple organic acids on aluminum hydroxide, *Journal of Environmental Sciences*, 19 (2007) 438-443.
- [66] J.P. Coates, The interpretation of infrared spectra: Published reference sources, *Applied spectroscopy reviews*, 31 (1996) 179-192.

- [67] G. Socrates, *Infrared and Raman characteristic group frequencies: tables and charts*, John Wiley & Sons 2004.
- [68] C. Bilton, F.H. Allen, G.P. Shields, J.A. Howard, Intramolecular hydrogen bonds: common motifs, probabilities of formation and implications for supramolecular organization, *Acta Crystallographica Section B: Structural Science*, 56 (2000) 849-856.
- [69] F.H. Allen, W.S. Motherwell, *Applications of the Cambridge Structural Database in organic chemistry and crystal chemistry*, *Acta Crystallographica Section B: Structural Science*, 58 (2002) 407-422.
- [70] E. Khan, A. Badshah, R. Kempe, Synthesis and Molecular Structure of Bis (4-methylpiperidino-dithiocarbamate) nickel (II), *Journal of the Chemical Society of Pakistan*, 32 (2010) 349-352.
- [71] E. Khan, U.A. Khan, A. Badshah, M.N. Tahir, A.A. Altaf, Supramolecular dithiocarbamate-gold (III) complex a potential DNA binder and antioxidant agent, *Journal of Molecular Structure*, 1060 (2014) 150-155.
- [72] Z. Gul, N.U. Din, E. Khan, F. Ullah, M.N. Tahir, Synthesis, molecular structure, anti-microbial, anti-oxidant and enzyme inhibition activities of 2-amino-6-methylbenzothiazole and its Cu (II) and Ag (I) complexes, *Journal of Molecular Structure*, 1199 (2020) 126956.
- [73] M. Oruganti, S.K. Nechipadappu, P.A. Khade, D.R. Trivedi, Solid-state versatility of the molecular salts/cocrystals of 2-Chloro-4-nitrobenzoic acid: a case study on halogen bonds, *ACS omega*, 2 (2017) 7146-7162.
- [74] R.G. Parr, L.v. Szentpaly, S. Liu, Electrophilicity index, *Journal of the American Chemical Society*, 121 (1999) 1922-1924.
- [75] P. Chattaraj, D. Roy, *Perennial Review: Update 1 of Chem. Rev.* 106, 2065 (2006), *Chem. Rev.* 107 (2007).
- [76] R. Parthasarathi, J. Padmanabhan, M. Elango, V. Subramanian, P. Chattaraj, Intermolecular reactivity through the generalized philicity concept, *Chemical physics letters*, 394 (2004) 225-230.
- [77] S. Saravanan, V. Balachandran, Quantum mechanical study and spectroscopic (FT-IR, FT-Raman, UV-Visible) study, potential energy surface scan, Fukui function analysis and HOMO-LUMO analysis of 3-tert-butyl-4-methoxyphenol by DFT methods, *Spectrochimica Acta Part A: Molecular and Biomolecular Spectroscopy*, 130 (2014) 604-620.

- [78] R. Parr, RGP-J. of the AC Society, and undefined 1983, “, Absolute hardness: companion parameter to absolute electronegativity,” ACS Publ, 105 (1983) 7512-7516.
- [79] R. Parr, R. Donnelly, M. Levy, W. Palke, Nanoscience and computational chemistry: Research progress, J. Chem. Phys, 68 (1978) 3801-3807.
- [80] P. Politzer, D.G. Truhlar, Chemical applications of atomic and molecular electrostatic potentials: reactivity, structure, scattering, and energetics of organic, inorganic, and biological systems, Springer Science & Business Media 2013.
- [81] T. Koopmans, The classification of wave functions and eigen-values to the single electrons of an atom, Physica, 1 (1934) 104-113.
- [82] R. Bader, A quantum theory, Clarendon: Oxford, UK, (1990).
- [83] R.F. Bader, H. Essén, The characterization of atomic interactions, The Journal of chemical physics, 80 (1984) 1943-1960.
- [84] S.J. Grabowski, QTAIM characteristics of halogen bond and related interactions, The Journal of Physical Chemistry A, 116 (2012) 1838-1845.
- [85] F. Fuster, S.J. Grabowski, Intramolecular hydrogen bonds: the QTAIM and ELF characteristics, The Journal of Physical Chemistry A, 115 (2011) 10078-10086.
- [86] P.S.V. Kumar, V. Raghavendra, V. Subramanian, Bader’s theory of atoms in molecules (AIM) and its applications to chemical bonding, Journal of Chemical Sciences, 128 (2016) 1527-1536.

Graphical abstract



Reaction between 2-amino-3-methylpyridine, 2-amino-4-methylbenzothiazole with salicylic acid, and 2-amino-5-chloropyridine with 3-chlorobenzoic acid were carried out and respective heterosynthons **1-3** were isolated. Structural elucidation of all compounds was carried out with the help of FT-IR and X-ray Diffraction for single crystals. Experimental data was validated by DFT and noncovalent interactions are discussed in full detail.